Dissolved iron in the Arctic shelf seas and surface waters of the central Arctic Ocean

Klunder, M. B.; Bauch, D.; Laan, P.; de Baar, H. J. W.; van Heuven, S.; Ober, S.

Published in:
Journal of geophysical research-Oceans

DOI:
10.1029/2011JC007133

Publication date:
2012

Dissolved iron in the Arctic shelf seas and surface waters of the central Arctic Ocean: Impact of Arctic river water and ice-melt

M. B. Klunder,[1] D. Bauch,[2] P. Laan,[1] H. J. W. de Baar,[1,3] S. van Heuven,[3] and S. Ober[4]

Received 17 March 2011; revised 27 October 2011; accepted 4 November 2011; published 31 January 2012.

[1] Concentrations of dissolved (<0.2 μm) Fe (DFe) in the Arctic shelf seas and in the surface waters of the central Arctic Ocean are presented. In the Barents and Kara seas, near-surface DFe minima indicate depletion of DFe by phytoplankton growth. Below the surface, lower DFe concentrations in the Kara Sea (~0.4–0.6 nM) than in the Barents Sea (~0.6–0.8 nM) likely reflect scavenging removal or biological depletion of DFe. Very high DFe concentrations (>10 nM) in the bottom waters of the Laptev Sea shelf may be attributed to either sediment resuspension, sinking of brine or regeneration of DFe in the lower layers. A significant correlation ($R^2 = 0.60$) between salinity and DFe is observed. Using $\delta^{18}O$, salinity, nutrients and total alkalinity data, the main source for the high (>2 nM) DFe concentrations in the Amundsen and Makarov Basins is identified as (Eurasian) river water, transported with the Transpolar Drift (TPD). On the North American side of the TPD, the DFe concentrations are low (<0.8 nM) and variations are determined by the effects of sea-ice meltwater, biological depletion and remineralization and scavenging in halocline waters from the shelf. This distribution pattern of DFe is also supported by the ratio between unfiltered and dissolved Fe (high (>4) above the shelf and low (<4) off the shelf).

Citation: Klunder, M. B., D. Bauch, P. Laan, H. J. W. de Baar, S. van Heuven, and S. Ober (2012), Dissolved iron in the Arctic shelf seas and surface waters of the central Arctic Ocean: Impact of Arctic river water and ice-melt, *J. Geophys. Res.*, *117*, C01027, doi:10.1029/2011JC007133.

1. Introduction

[2] The Arctic Ocean is linked to the global thermohaline circulation, mainly through a strong contribution of Arctic Ocean waters to North Atlantic Deep Water [*Rudels*, 2001]. Due to ice cover and harsh conditions, the Arctic Ocean is one of the least studied oceans, and knowledge of the trace metal distributions of the Arctic Ocean is very limited. In contrast to other world Oceans, the Arctic Ocean is characterized by vast continental shelves (over 1/3 of the total Arctic Ocean area) and by a strong (seasonal) input of freshwater to surface waters from Siberian rivers (Ob, Yenisey, Lena) and North American rivers (Mackenzie) and by seasonal ice-melt [*Aagaard et al.*, 1981]. This freshwater causes a strong density difference between the mixed layer and deeper waters, which limits winter convection [*Rudels*, 2001]. These physical circumstances are expected to affect the distribution of dissolved iron (DFe) in the water column of the Arctic, resulting in a deviation from the vertical distribution common to open ocean profiles [*Johnson et al.*, 1997; *Moore and Braucher*, 2008]. Instead, in the Arctic Ocean, the strong lateral DFe supply into the stratified surface layers and relatively little vertical mixing are expected to result in high DFe concentrations in the surface layers, relative to lower concentrations at depth.

[3] In other regions in the global ocean, Fe availability has been shown to be of vital importance to phytoplankton growth [*Martin and Gordon*, 1988; *de Baar et al.*, 1995; *Boyd et al.*, 2000]. In the Arctic, despite low temperatures and relatively low light levels, significant primary production is reported, most notably on the vast Arctic shelves [*Carmack and Wassmann*, 2006; *Arrigo et al.*, 2008]. Recently more has become known about the role of light, temperature and nutrients in primary production in the Arctic Ocean [*Gosselin et al.*, 1997; *Pabi et al.*, 2008]. However, little is still known about the distribution of DFe and the role of DFe in Arctic primary production. A study by *Measures* [1999] showed reactive (unfiltered) Fe concentrations in the 1–4 nM range in the upper mixed layer over the central Arctic Ocean. They attributed these relatively high concentrations to melting of sea-ice with entrained sediments. Indeed, *Nürnberg et al.* [1994] have shown the importance of sediment entrainment in sea-ice for transport of sediment from Arctic rivers to the central Arctic Ocean. Therefore the mechanism of melting of

[1]Biological Oceanography, Netherland Institute for Sea Research, Den Burg, Netherlands.
[2]Ocean Circulation and Climate Dynamics, GEOMAR, Helmholtz Centre for Ocean Research, Kiel, Germany.
[3]Department of Ocean Ecosystems, University of Groningen, Groningen, Netherlands.
[4]Physical Oceanography, Netherland Institute for Sea Research, Den Berg, Netherlands.

0148-0227/12/2011JC007133

sediment laden sea-ice is a possible DFe source to the central Arctic. Mass balance models using $\delta^{18}O$, salinity and nutrients showed that fluvial input sources significantly affect the surface waters of the central Arctic, which comprises about 5–15% river water [*Bauch et al.*, 1995; *Ekwurzel et al.*, 2001]. Model calculations indicate that river water in the Eurasian Basin is of Siberian origin [*Harms et al.*, 2000]. Moreover, based on Ba concentrations from the same cruise as ours, T. Roeske et al. (Utility of dissolved Ba in distinguishing North American from Eurasian runoff and in the light of its part in biogeochemical cycling of the Arctic Ocean, manuscript submitted to *Marine Chemistry*, 2011) conclude that the observed river water is of Eurasian origin. Because DFe in the Siberian rivers is 2–3 orders of magnitude higher than common open ocean surface concentrations [*Dai and Martin*, 1995; *Gebhardt et al.*, 2005; *Hölemann et al.*, 2005; *Moore and Braucher*, 2008], even a small portion of the DFe in this water escaping the relatively high Arctic scavenging removal regime [*Cai et al.*, 2010] could strongly affect surface DFe concentrations in the central Arctic Ocean.

[4] In this paper we present the distribution of DFe on the Arctic shelves (Barents, Kara and Laptev seas) and in the surface waters (upper 250 m) of the central Arctic, obtained during the ARK XXII/2 expedition of R/V *Polarstern* in August–September 2007 (Figure 1). The multicomponent approach using $\delta^{18}O$, salinity and nutrients as well as total alkalinity (A_T) measurements taken during the same cruise [see also *Bauch et al.*, 2011] is used to study the influence of the different freshwater sources on the DFe distribution in the upper Arctic Ocean waters. The distribution of DFe in the deep waters of the central Arctic Ocean is presented in a complementary manuscript by M. B. Klunder et al. (Dissolved Fe in the Arctic Ocean: Important role of hydrothermal sources, shelf input and scavenging removal, submitted to *Journal of Geophysical Research*, 2011).

2. Material and Methods

2.1. Sampling and Analysis

[5] Water samples were collected during the ARK XXII/2 expedition of R/V *Polarstern* between 1 August and 23 September 2007 (Figure 1). At discrete depths, samples were taken using 24 internally Teflon coated PVC 12 L GO-FLO samplers (General Oceanics, Inc.) mounted on a Titanium frame, which was connected to a Kevlar hydrowire [*de Baar et al.*, 2008]. Inside a class 100 clean room environment samples for DFe analysis were collected from the GO-FLO bottles [*de Baar et al.*, 2008]. Seawater was filtered using a 0.2 μm filter cartridge (Sartrobran-300, Sartorius) under nitrogen pressure. For each depth replicate samples of DFe were taken in 60 ml High Density Polyethylene (HDPE) sample bottles and acidified to pH = 1.8 with 12 M HCl (Baseline, Seastar Chemicals). Previously, all bottles, used for storage of reagents and samples, were acid cleaned according to a three step cleaning procedure, as described by *Middag et al.* [2009].

[6] The DFe was measured using flow injection analysis with luminol chemiluminescence, where samples were buffered in-line to pH = 4, using a 0.12 M ammonium acetate buffer (pH = 6.5). The DFe was preconcentrated on an IDA Toyopearl AF-Chelate resin [*Klunder et al.*, 2011]. After preconcentration, the column was rinsed (60 s) with ultrapure type 1 water and subsequently Fe was eluted from the column (120 s) using 0.4 M HCl (Merck Suprapur). Preconcentration time was usually 120 s, except for the Laptev Sea stations, where a short loading time (15 s) enabled determination of the very high concentrations present at this location.

2.2. Calibration and Validation

[7] The system was calibrated using standard additions of Fe to low DFe seawater. If an outlying value for DFe was observed, the profiles of the other trace metals (dissolved aluminum (DAl) and manganese (DMn)) and other nutrients (silicic acid, nitrate and nitrite, phosphate) were evaluated for consistency with the regarded data point. In the case that no deviations were observed in the other parameters and both the initial and duplicate sample showed an exceptional value, the exceptional data point was considered as erroneous if the value deviated more than +25% from the expected profile based linear interpolation between the DFe-concentration above and below the data point [after *Middag et al.*, 2009; *Klunder et al.*, 2011]. The total number of data points for DFe during ARK XXII/2 was 785. In total 5 data points were rejected, of which only 2 data points were situated in Arctic surface waters. Data Set S1 including stations, positions, date, depth, nutrient data, DFe data and total alkalinity is available in the auxiliary material.[1] The blank is the background concentration of DFe in ultrapure type 1 water and chemicals and is defined as the concentration measured at 0 s loading time; the blank was 0.02 $\pm$ 0.02 nM (n = 41) on average and did not exceed 0.075 nM. The detection limit (3σ of the blank) was 0.07 nM or 70 pM. The amount of Fe added to sample by addition of 12 M HCl (Baseline, Seastar) is <0.4 pM per sample and is considered negligible [*Klunder et al.*, 2011].

[8] The accuracy of the Fe flow injection analysis system was verified by regularly analyzing SAFe D2 standard seawater. The results agreed well with the community consensus values: 0.92 $\pm$ 0.057 nM, n = 24. (Certified consensus value is 0.92 $\pm$ 0.03 (http://www.geotraces.org/)).

2.3. Other Variables

[9] Samples for dissolved Mn (DMn) and dissolved Al (DAl) were simultaneously sampled with those for DFe [*Middag et al.*, 2011, 2009]. At some stations, besides the Fe in the dissolved fraction presented here, Fe was also measured in a smaller size fraction (<1000 kDa) and a "total dissolvable" fraction (unfiltered) [*Thuroczy et al.*, 2011]. Salinity and potential temperature data were taken from the CTD profile.

[10] Total alkalinity (A_T) was determined by potentiometric titration in an open cell, according to the procedures outlined by *Dickson et al.* [2007]. Samples were collected in 250 ml borosilicate bottles and poisoned with 100 μl of a 50% saturated solution of $HgCl_2$ (i.e., to a concentration of 0.02%) and stored dark and cool, but without freezing, until analysis. All samples were analyzed during the expedition, most within 24 h after sampling, with only a few stations within 72 h of sampling. A correction factor of 1.0002 was

[1] Auxiliary material data sets are available at ftp://ftp.agu.org/apend/jc/2011jc007133. Other auxiliary material files are in the HTML. doi:10.1029/2011JC007133.

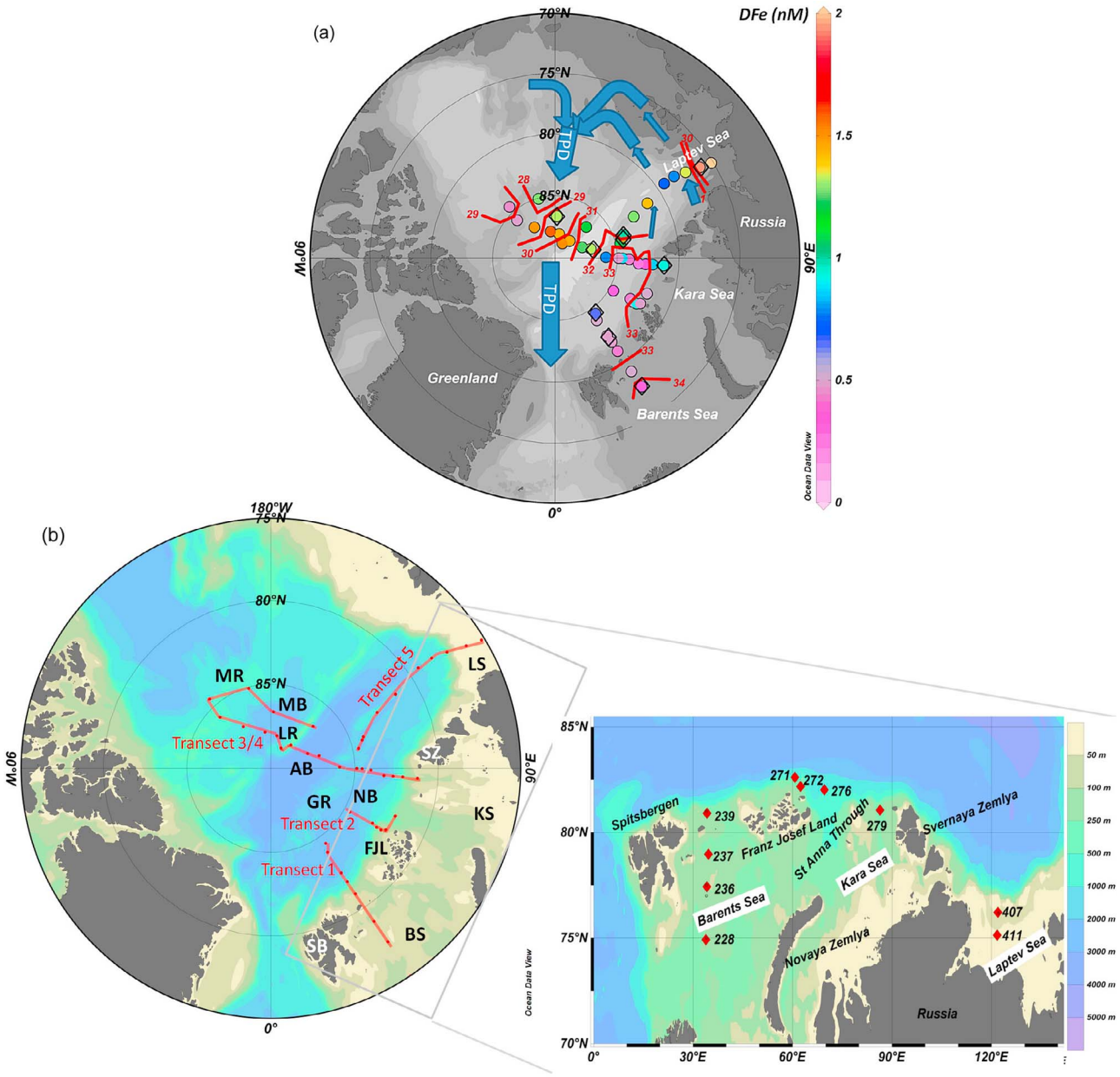

Figure 1. (a) Station map of all stations occupied during ARK XXII/2. Color scale indicates dissolved Fe averages of surface layer waters (SLW). Stations measured for total Fe (TFe) are marked with diamonds. Average salinity isolines of the surface layer waters are shown in red. Blue arrows indicate the transpolar drift (schematically, after *Rudels* [2001]). NB, Nansen Basin; AB, Amundsen Basin; MB, Makarov Basin. (b) Map of the Arctic Ocean with the transects and shelf stations occupied during ARK XXII/2. The gray square in the overview marks the position of the enlargement for the Arctic shelves. BS, Barents Sea; FJL, Franz Josef Land; BS, Barents Sea; KS, Kara Sea; LS, Laptev Sea; NB, Nansen Basin; GR, Gakkel Ridge; AB, Amundsen Basin; LR, Lomonosov Ridge; MB, Makarov Basin; MR, Mendeleev Ridge.

applied to the results to compensate for the diluting effect of adding the $HgCl_2$ solution. Precision of the analysis, defined as the standard deviation of differences between duplicate analyses of certified reference material (CRM, batch 76, distributed by the Scripps Institution of Oceanography [*Dickson*, 2001]) is 1.5 μmol kg^{-1} (n = 68). Analyses of CRM showed an initial bias of the instrument of about +0.3% (i.e., about 6 μmol kg^{-1}), which over the course of the cruise decreased to about +0.1% (i.e., about 2 μmol kg^{-1}). This minor inaccuracy and the gradual drift therein are corrected for in the results. The final data set of A_T is accurate to ± 4 μmol kg^{-1}, this being approximately twice the standard deviation of the CRM measurements after the correction for bias and drift is performed.

[11] Oxygen isotopes were analyzed at the Leibniz Laboratory (Kiel, Germany) applying the CO_2-water isotope equilibration technique on a Finnigan gas bench II unit coupled to a Finnigan Delta Plus XL. At least 2 subsamples were

analyzed to reach an overall measurement precision for all $\delta^{18}O$ analysis of at least $\pm 0.03‰$ or smaller. For further details see *Bauch et al.* [2011]. The $^{18}O/^{16}O$ ratio is given versus VSMOW in the usual δ-notation [*Craig*, 1961].

2.4. Calculation of River Water and Sea-Ice Meltwater Fractions

[12] Stable oxygen isotopes of the water in conjunction with salinity have proven to be a useful and reliable tracer to identify and distinguish freshwater sources [*Östlund and Hut*, 1984]. Moreover, Atlantic and Pacific-derived waters within the marine fraction can be distinguished and quantified based on nutrient concentrations [*Ekwurzel et al.*, 2001; *Jones et al.*, 1998, 2008; *Yamamoto-Kawai et al.*, 2008]. The water mass fractions are calculated using either a three component or a four-component system of mass balance equations based on salinity, $\delta^{18}O$, and PO_4^*. The latter PO_4^* represents the initial phosphate concentration that accounts for organic respiration of dissolved oxygen and is defined as $PO_4^* = PO_4^{3-} + O_2/175 - 1.95\ \mu mol\ kg^{-1}$ [*Broecker et al.*, 1985]. In deep waters and below a closed sea-ice cover at reduced O_2 air/sea exchanges, the PO_4^* is a quasi-conservative tracer [*Ekwurzel et al.*, 2001]. The overall mass balance is governed by the following equations [*Ekwurzel et al.*, 2001]:

$$f_a + f_p + f_i + f_r = 1, \tag{1}$$

$$f_a S_a + f_p S_p + f_i S_i + f_r S_r = S_{meas}, \tag{2}$$

$$f_a \delta^{18}O_a + f_p \delta^{18}O_p + f_i \delta^{18}O_i + f_r \delta^{18}O_r = \delta^{18}O_{meas}, \tag{3}$$

$$f_a PO^*_{4a} + f_p PO^*_{4p} + f_i PO^*_{4i} + f_r PO^*_{4r} = PO^*_{4meas}, \tag{4}$$

where f_a is the fraction of Atlantic water, f_p the fraction of Pacific-derived water, f_i the fraction of sea-ice meltwater (or brine influence if f_i is negative), and f_r is the fraction of meteoric water for which the $\delta^{18}O$ signal is a suitable indicator. Meteoric water is all water ultimately due to precipitation. In the Arctic Ocean, this can be supplied as river water or as local net precipitation. River water and local precipitation are isotopically identical but river water exceeds net precipitation [*Serreze et al.*, 2006], therefore we refer to this fraction as river water. The S, O and PO_4^* with the corresponding subscripts are the end-member values and measured values of salinity, $\delta^{18}O$ and PO_4^* [see *Bauch et al.*, 2011]. In the Atlantic regime calculated fractions of Pacific-derived waters may be strongly negative, because of end-member uncertainties and also due to a nonconservative behavior of dissolved oxygen near the surface. In these cases, Pacific-derived water can be assumed to be absent and a 3-component system of equations is solved (equations (1)–(3) with f_p set to zero). An alternative calculation (similar to equations (1)–(4)) using nitrate to phosphate ratios (N/P) facilitates the differences in nitrate levels between Atlantic and Pacific-derived waters [*Jones et al.*, 1998, 2008; *Yamamoto-Kawai et al.*, 2008]. Comparison of Pacific-derived fractions from PO_4^* and N/P-based calculations are especially important for the interpretation of station data on the Canadian Side of the Transpolar Drift (stations 338, 342, and 345; Figure 5). While the PO_4^* approach generally tends to underestimate Pacific-derived waters due to nonconservative behavior O_2 near the surface, the N/P approach in the Transpolar Drift contains a seemingly Pacific signal that in fact is originating from denitrification processes along the Siberian shelves [*Bauch et al.*, 2011].

[13] A negative sea-ice meltwater fraction reflects the amount of water removed by sea-ice formation and the absolute value is proportional to the subsequent addition of brines to the remaining water column. All fractions are net values reconstructed from the $\delta^{18}O$ and salinity signature of each sample and are the result of time integrated effects on the sample volume over the residence time of the water. Uncertainties based on analytical errors are considerably smaller than systematic and conceptual errors arising from limited knowledge of end-member values. Systematic errors based on uncertainties in end-member salinity and $\delta^{18}O$ data remain mostly within $\pm 1\%$ for river water and sea-ice meltwater fractions and uncertainties for Pacific water fraction are up to about 10% for the PO_4^*-based calculation [*Ekwurzel et al.*, 2001] and up to 10% for the N/P-based method [*Yamamoto-Kawai et al.*, 2008]. For a detailed discussion see *Bauch et al.* [2011].

3. Hydrographic Background

[14] The largest inflow into the Arctic Ocean is Atlantic water, marked by high potential temperatures (θ) ($\sim$3–5°C) and high salinity ($\sim$35) [*Rudels*, 2001]. This Atlantic water enters the Arctic Ocean in two branches. One branch flows through the Fram Strait and then eastward along the Siberian continental margin at a depth of $\sim$200–600 m [*Rudels*, 2001]. The other branch flows over the Barents Sea and Kara Sea and joins the Fram Strait Branch at St. Anna Trough [*Rudels*, 2001]. The dominant surface current across the central Arctic Ocean is the Transpolar Drift (TPD), fed by surface waters from the Laptev and East Siberian seas. The TPD crosses the central Arctic Ocean, and leaves the basin southward through Fram Strait and there constitutes forms the East Greenland Current [*Rudels*, 2001; Figure 1a].

[15] Throughout the Arctic, the upper surface waters are strongly influenced by a major freshwater input from the Siberian and North American rivers, by Pacific inflow through Bering Strait and by melting of sea-ice [*Aagaard and Carmack*, 1989]. This results in a surface mixed layer (SML) marked by minima of salinity and potential temperature. During ARK XXII/2, the mixed layer (defined as the shallowest depth deeper than 10 m where σ-$\sigma_{10m} < 0.05$ [after *Rintoul et al.*, 2001]) varies between 11 and 25 m over the study area. During the Ultraclean CTD casts, in many cases the shallowest sample measured was situated below the SML. Below the SML, upper halocline waters (UHW) are marked by a nutrient maximum and are most pronounced in the Makarov Basin at salinities of about 32.5–33.5 [e.g., *Guay and Kenison Falkner*, 1997]. The lower halocline waters (LHW), observed in all Arctic basins, are originally formed by winter convection in the Nansen Basin [*Rudels et al.*, 2004] and intrusions of saline shelf water [*Steele and Boyd*, 1998], causing higher salinities 34–34.5 [e.g., *Guay and Kenison Falkner*, 1997] compared to the UHW. *Steele and Boyd* [1998] mention the formation of halocline waters in the Makarov Basin as a result of large amounts of

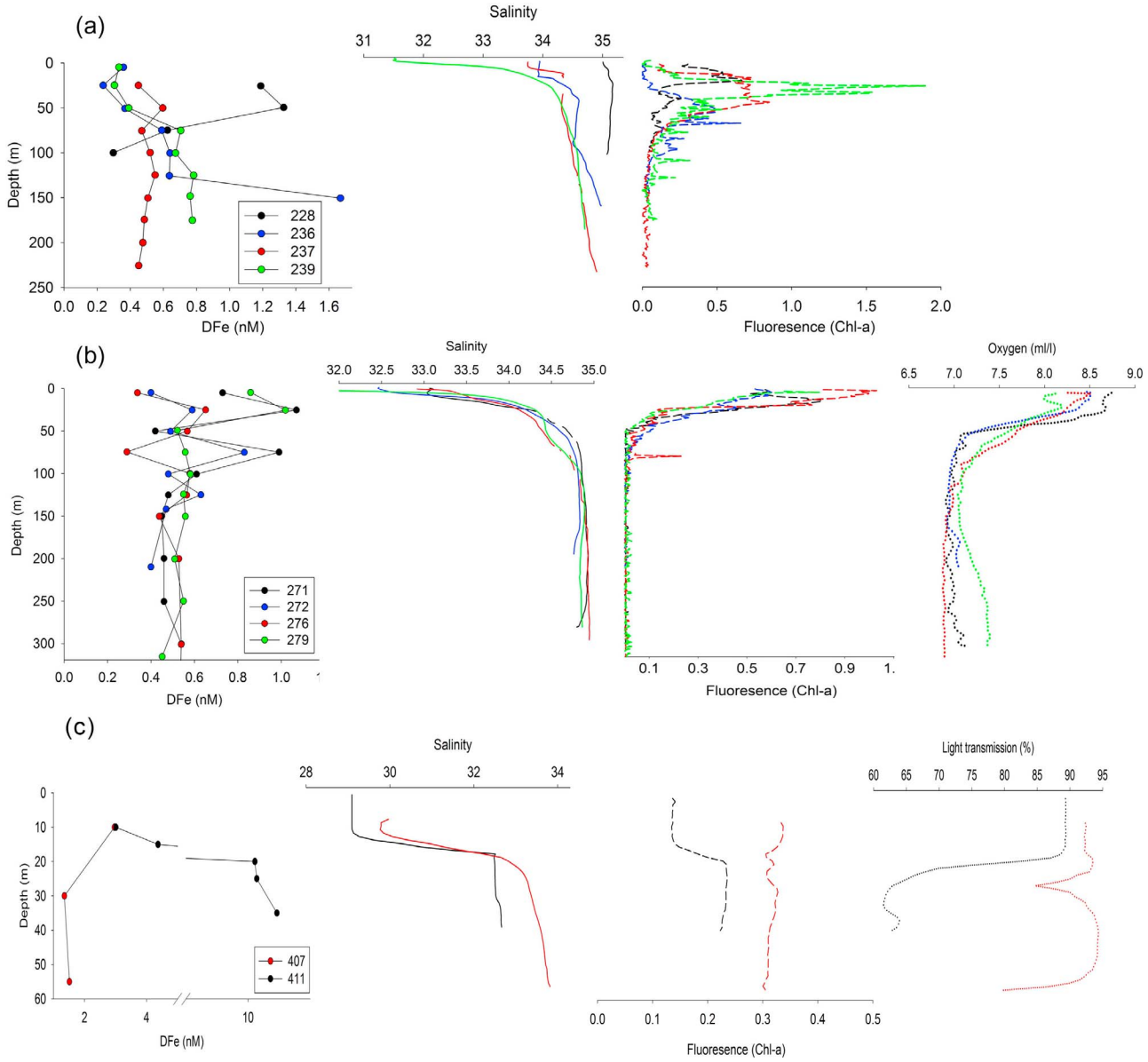

Figure 2. Depth profiles of DFe, salinity and fluorescence (indicative of Chl-a; arbitrary units) for the stations on the (a) Barents Sea Shelf, (b) Kara Sea Shelf and (c) the Laptev Sea Shelf (see Figure 1b). For clarification of the discussion, for the Kara Sea shelf, also oxygen profiles are shown (see text) and for the Laptev Sea shelf also light transmission data is shown (see text). Station profiles for salinity, fluorescence, light transmission and oxygen follow the same colors as indicated in the DFe profile for each region.

freshwater leaving the Laptev Shelf Continental Margin. Below the halocline, Atlantic derived waters are observed, marked by a temperature maximum and higher salinity of about 34.92 in the southwestern Nansen Basin [*Aagaard et al.*, 1981]. In this study, the surface layer waters (SLW) comprise the SML, UHW and LHW and are defined as waters with salinity <34.5 [after *Guay and Kenison Falkner*, 1997].

4. Results

[16] For all stations occupied during ARK XXII/2, the average DFe concentrations in the SLW together with isohalines are shown in Figure 1a. Positions of transects are depicted in Figure 1b. Since there is a clear correlation between DFe and salinity in the upper Arctic Ocean, the fractions of the different freshwater sources are displayed together with DFe (Figures 3–6) as they may give information about the different sources of Fe in the Arctic Ocean.

4.1. Shelf Seas

[17] For the shelf seas, depth profiles of DFe, together with light transmission and salinity, are depicted in Figure 2. In the Barents Sea (Figures 2a and 3) high Fe (>1 nM) and salinity (>35.1) was found in the upper layer (25–50 m) southernmost station (station 228). Below a DFe enrichment in surface waters, stations 236 and 239 showed a subsurface minimum at ~50 m water depth (also at station 237), which

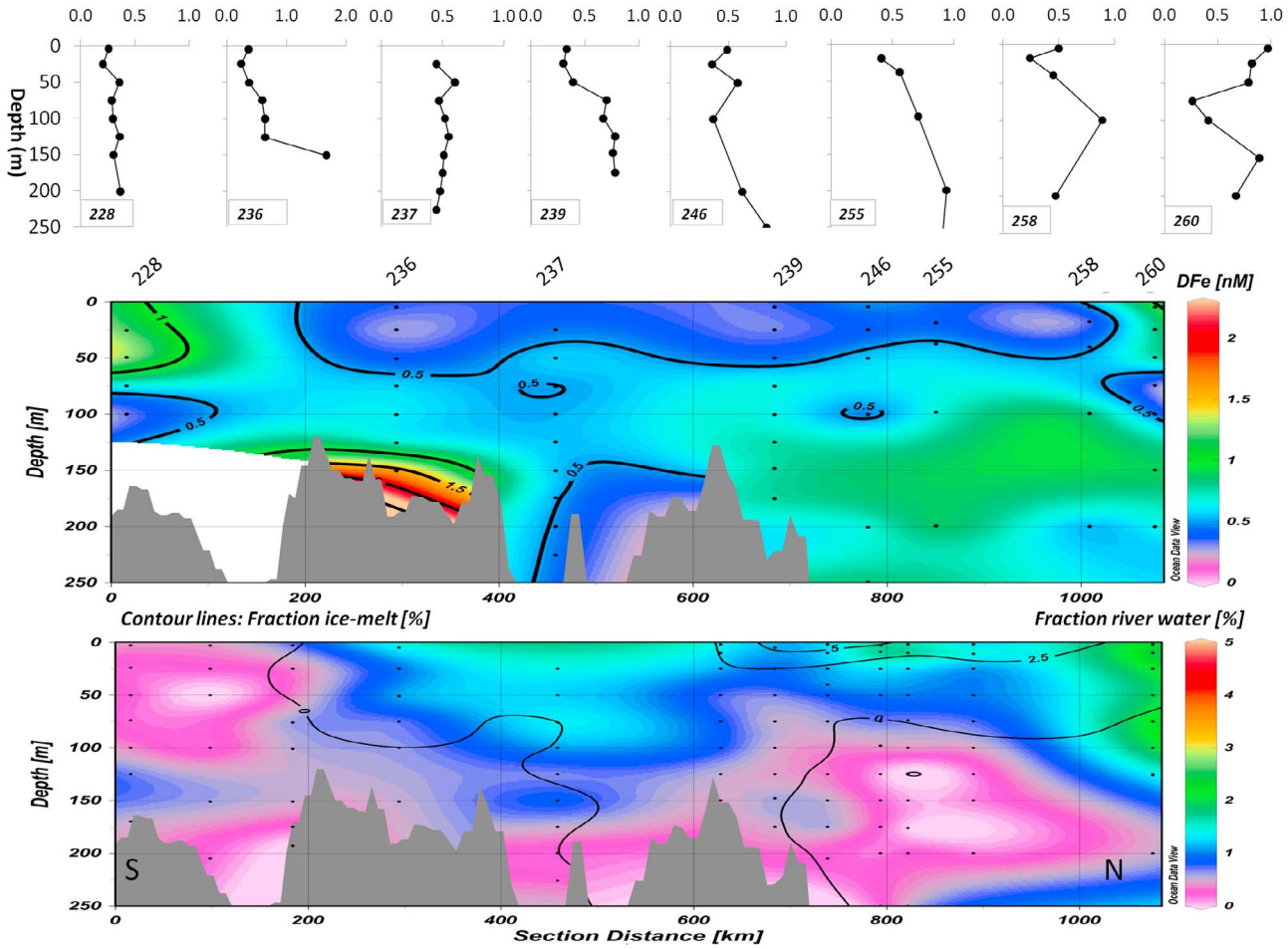

Figure 3. (top) Dissolved Fe depth profiles, (middle) dissolved Fe transect plot and (bottom) transect plot of river water fractions (color) and sea-ice meltwater fractions (contours) in the upper 250 m of the water column at transect 1 (see Figure 1b). Station numbers of transects are indicated above Figure 3 (middle) and South (S) and North (N) orientation within Figure 3 (bottom). Note the different scale for the DFe depth profiles. (Gridding: DIVA gridding (ODV); 72 × 72 (Figure 3, middle) and 60 × 60 (Figure 3, bottom).)

corresponded to a maximum of fluorescence. Below 50 m, the DFe concentrations were relatively constant with depth (0.6–0.8 nM). The fractions of river water were relatively low in the Barents Sea and some sea-ice meltwater was observed in the upper water around station 239 (Figure 3).

[18] Four stations were occupied northeast of Franz Josef Land, over the St. Anna Trough and at the Kara Sea slope (Figure 1b and profiles in Figure 2b). All stations showed a surface depletion of DFe in the upper 10 m and a pronounced subsurface maximum at 25 m depth. At all stations this layer was marked by reduced temperature θ (not shown), relatively low salinity (<33.5), higher fluorescence (Figure 2b) and some river water (up to 3%) as well as sea-ice meltwater (2–5%) was observed (Figure 4). Below the DFe minimum at 25 m depth there was an enrichment at 75 m and below that a relatively low (0.4–0.5 nM) DFe concentrations (station 271/272) or a depletion at 75 m (station 276) and below that a relatively higher DFe (0.5–0.6 nM) (station 276/279).

[19] Two stations (407 and 411) were occupied in the shallow Laptev Sea (Figure 2c). In the upper 10 m the DFe concentrations of ~3 nM coincided with low salinity and correspondingly high fractions of river water (12–14%) and some sea-ice meltwater (~3%). Below the low salinity layer low DFe concentrations (<2 nM), sea-ice meltwater and river water contributions were found at station 407. At station 411, closer to the shelf edge, high DFe concentrations (>10 nM) corresponded to higher salinity and lower light transmission (Figure 2c), and a strong influence of brine waters (negative sea-ice meltwater fraction; fi ~ −9%). Relatively high river water fractions (~15%) were observed.

4.2. Surface Waters in the Central Arctic Basin

[20] There was a strong relation between high DFe and low salinity in the Eurasian Basin and central Arctic (Figure 1a), where in the southwestern Nansen Basin low concentrations of DFe corresponded to high salinity and in the Amundsen and Makarov Basins increasing DFe corresponded to decreasing salinity. An exception to this inverse correlation pattern between salinity and DFe was the region above the Alpha Ridge: here at stations 338 and 342 (Figure 1a), which we assume to be just outside the influence of the Transpolar Drift, salinity further decreased but also DFe concentrations were low. The position of the Transpolar Drift is inferred from the distribution of Pacific-derived waters and extrema

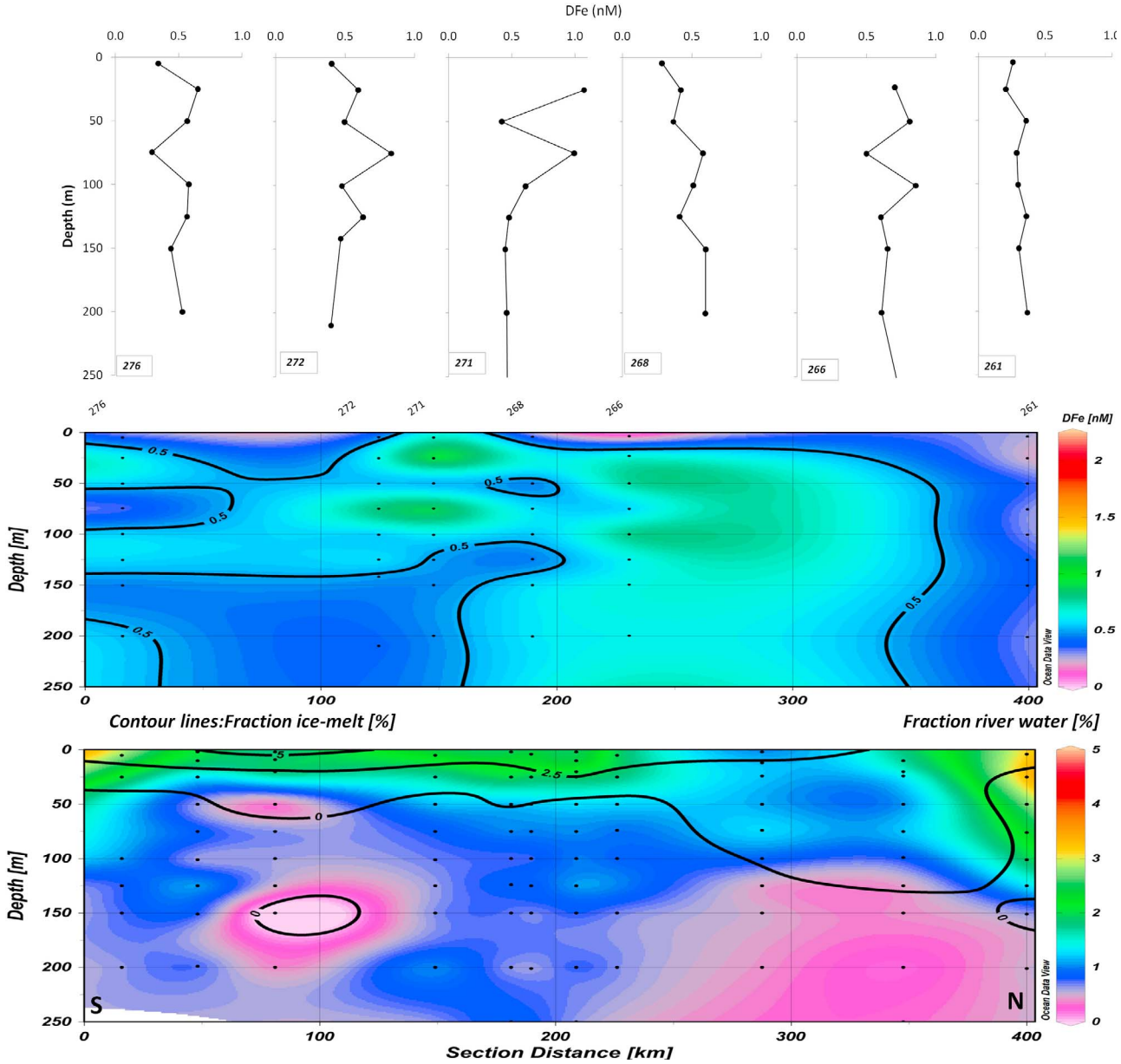

Figure 4. (top) Dissolved Fe depth profiles, (middle) dissolved Fe transect plot and (bottom) transect plot of river water fractions (color) and sea-ice meltwater fractions (contours) in the upper 250 m of the water column at transect 2 (see Figure 1b). Station numbers of transects are indicated above Figure 4 (middle) and South (S) and North (N) orientation within Figure 4 (bottom). Note the different scale for the DFe depth profiles. (Gridding: DIVA gridding (ODV); 90 × 90 (Figure 4, middle) and 60 × 60 (Figure 4, bottom).)

of river water and negative sea-ice meltwater fractions (see discussion by *Bauch et al.* [2011]). Moreover,the enhanced transport rates inferred from transient tracer evidence support this position of the TPD (M. Rutgers van der Loeff et al., Shelf-basin exchange times of Arctic surface waters estimated from $^{228}Th/^{228}Ra$ disequilibrium, submitted to *Journal of Geophysical Research*, 2011).

[21] In the western part of the Nansen Basin (Transects 1 and 2), the concentrations of DFe were generally low in the upper surface, despite some freshwater from sea-ice

Figure 5. (top) Dissolved Fe depth profiles, (middle) dissolved Fe transect plot and (bottom) transect plot of river water fractions (color) and sea-ice meltwater fractions (contours) in the upper 250 m of the water column at transect 3/4 (see Figure 1b). Station numbers of transects are indicated above Figure 5 (middle) and South (S) and North (N) orientation within Figure 5 (bottom). The different Basins are indicated by arrows below the transect plots. Note the different scale for the DFe depth profiles. The red bar in Figure 5 (bottom) indicates the region where water mass fractions are calculated using N/P ratio. (Gridding: DIVA gridding (ODV); 72 × 72 (Figure 5, middle) and 60 × 60 (Figure 5, bottom).)

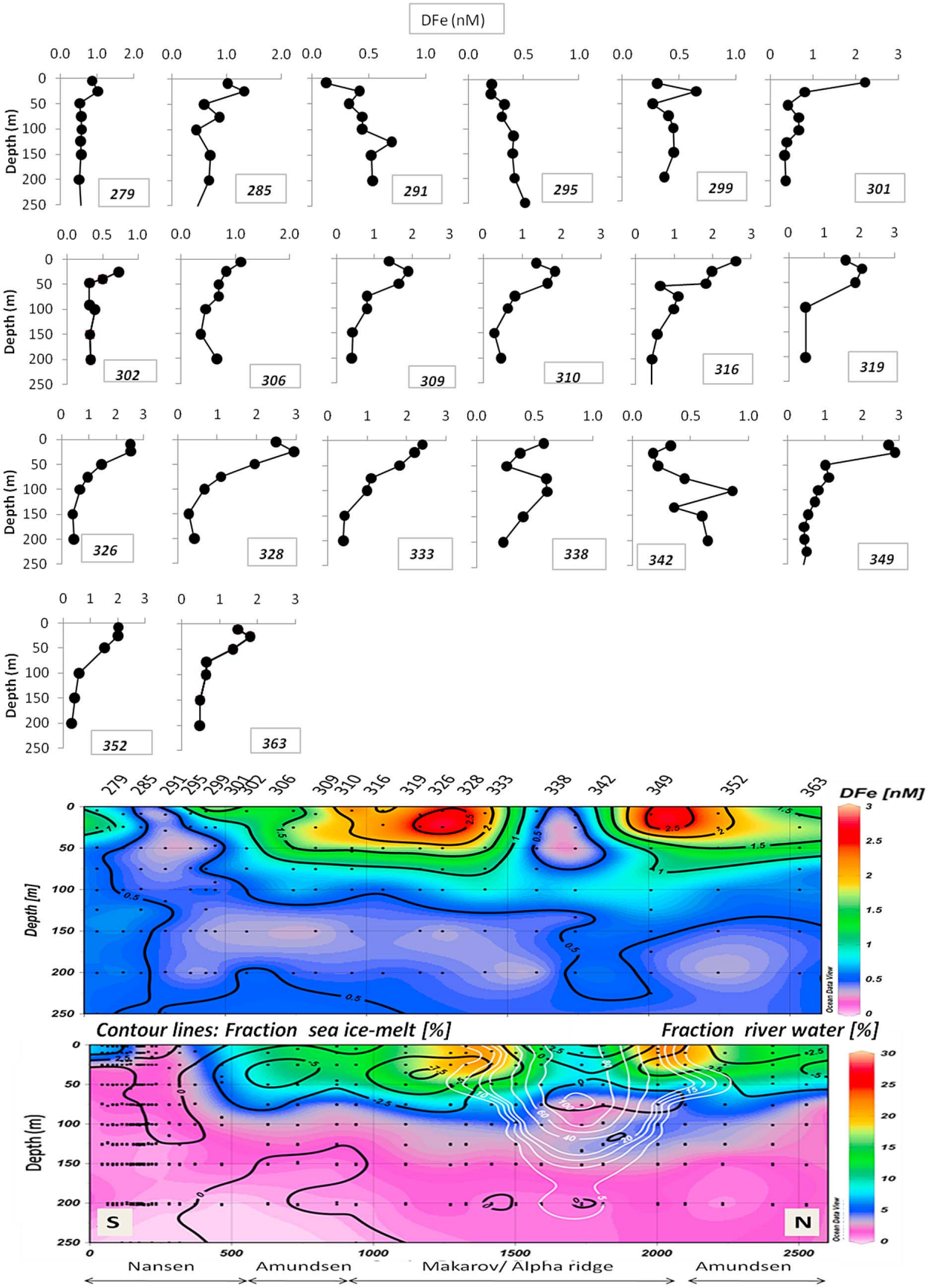
DFe (nM)
Depth (m)
279
285
291
295
299
301
302
306
309
310
316
319
326
328
333
338
342
349
352
363
DFe [nM]
Depth [m]
Contour lines: Fraction sea ice-melt [%]
Fraction river water [%]
Depth (m)
S
N
0
500
1000
1500
2000
2500
Nansen
Amundsen
Makarov/ Alpha ridge
Amundsen

Figure 5

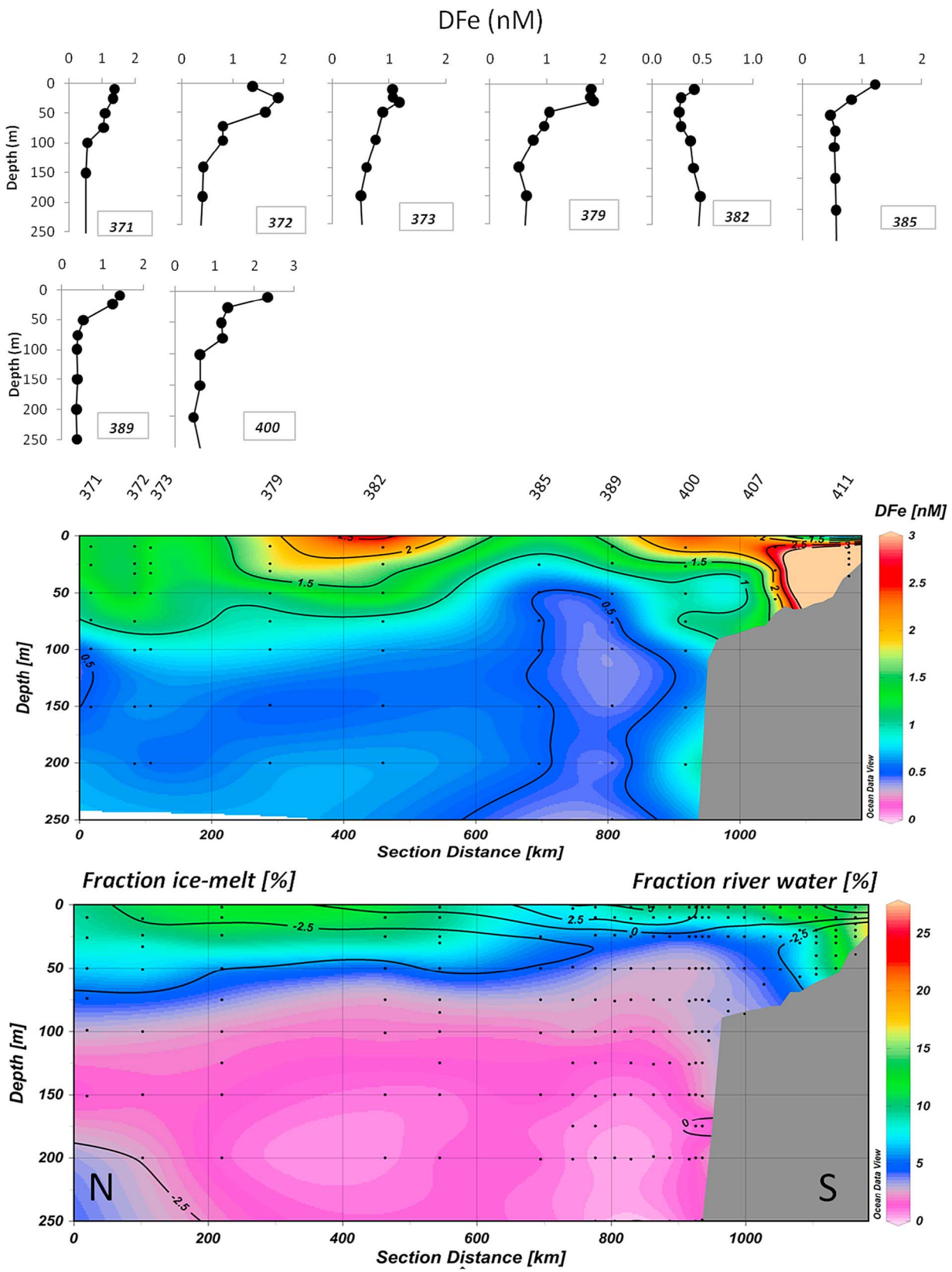

Figure 6. (top) Dissolved Fe depth profiles, (middle) dissolved Fe transect plot and (bottom) transect plot of river water fractions (color) and sea-ice meltwater fractions (contours) in the upper 250 m of the water column at transect 5 (see Figure 1b). Station numbers of transects are indicated above Figure 6 (middle) and South (S) and North (N) orientation within Figure 6 (bottom). Note the different scale for the DFe depth profiles. (Gridding: DIVA gridding (ODV); 72 × 72 (Figure 6, middle) and 60 × 60 (Figure 6, bottom).)

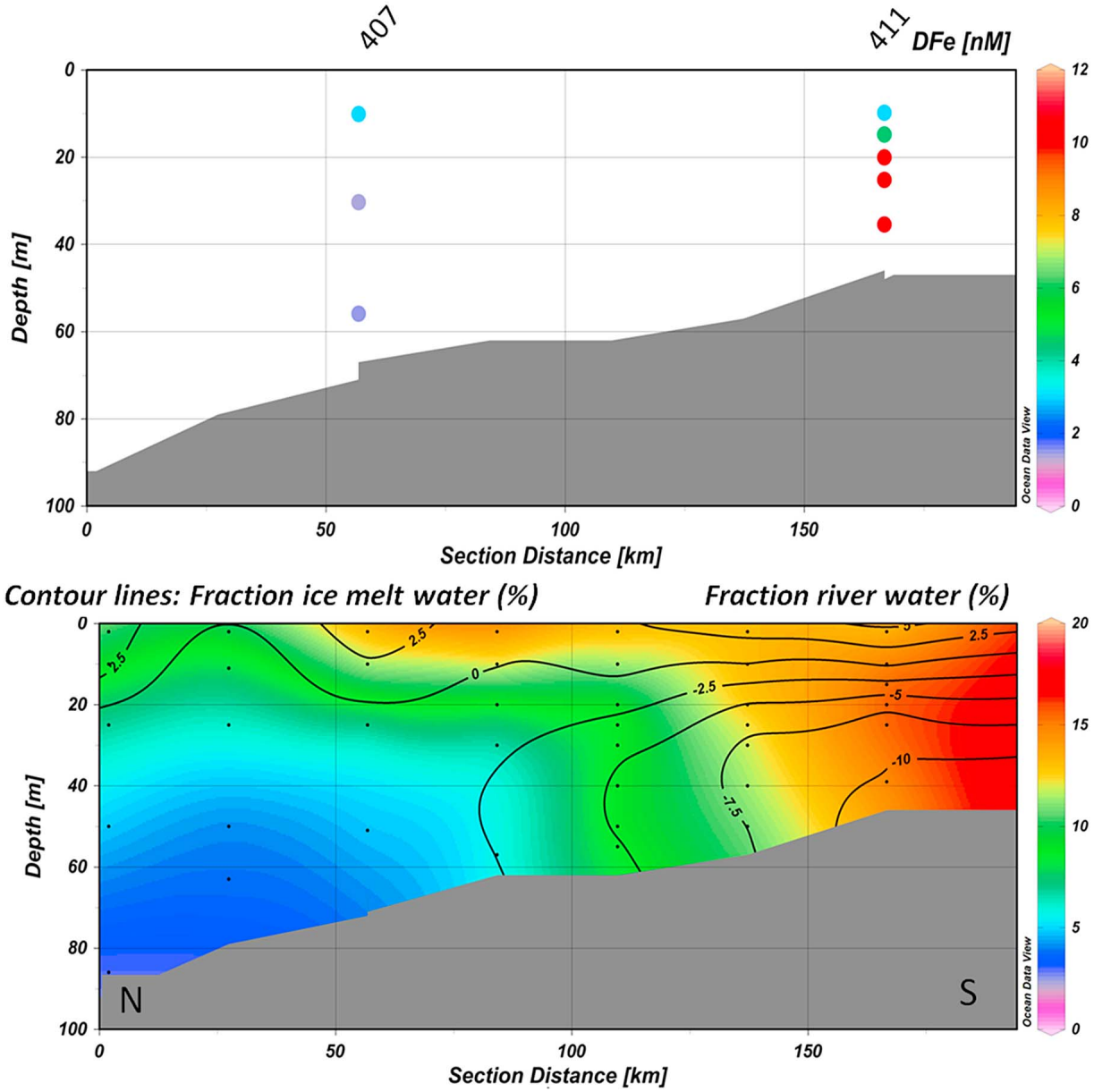

Figure 7. (top) Dissolved Fe data points plot and (bottom) transect plot of of river water fractions (color) and sea-ice meltwater fractions (contours) in the upper 250 m of the water column of the stations on the Laptev Shelf (see Figure 1b). Station numbers of transects are indicated above Figure 7 (top) and South (S) and North (N) orientation within Figure 7 (bottom). (Gridding: DIVA gridding (ODV); 60 × 60 (Figure 7, bottom).)

meltwater and river water (Figures 3 and 4). In the northernmost station of transect 1, the DFe increased with increasing river water (Figure 3), whereas further east, at the northernmost station of transect 2, high river water and low DFe was found (Figure 4). The western part of the Nansen Basin had relatively low fractions of river water and sea-ice meltwater (with a total always <6%) in the upper surface. Sea-ice meltwater was mostly restricted to the upper 25 m where DFe was generally low (<0.5 nM). Although river water was present (2–3%) over most of the western Nansen Basin, the river influence was very low (<1%) at the shelf break just north of Franz Josef Land (Figure 4).

[22] Further east at the Kara Sea slope, increasing river water fractions and about constant sea-ice meltwater fractions coincided with relatively higher DFe (Figure 4; ∼0–150 km of section). In the central Nansen Basin both the DFe concentrations (∼0.5 nM) and the river water fractions were relatively low (Figure 5; see section at ∼150–400 km).

[23] Relatively high surface DFe concentrations were observed above the Gakkel Ridge together with large fractions of river water and some influence of brine waters (i.e., negative sea-ice meltwater fractions) (Figure 6). In the Nansen Basin near the Laptev Sea margin, the surface DFe concentrations decreased as well as the fractions of river

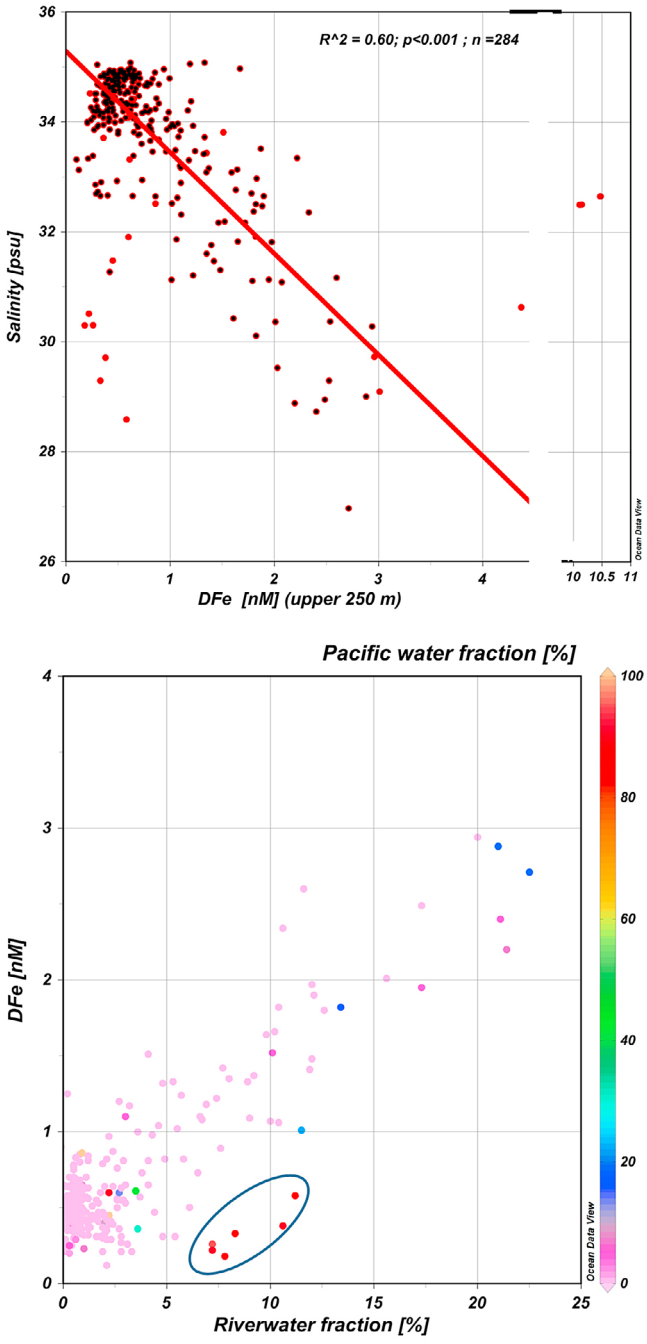

Figure 8. (top) Relation between DFe and salinity in the upper 250 m. Red dots show all data, black dots show all data points excluding stations 338/342 (see text section 5.4) and 407/411 (see text section 5.2). Correlation coefficient, p-value and N are given for the reduced data set (black dots). Note the break within the DFe axis. (bottom) Relation between the concentration of DFe (nM) and fraction of river water (%) for the whole water column in the central Arctic Ocean (shelf stations are excluded (Figure 1b)). Fraction of Pacific-derived water (%) is shown in color scale. The blue ellipse indicates the data points >50 m at stations 338 and 342 (see text for discussion).

water and sea-ice meltwater (Figure 6; ~600–800 km of section). Toward and onto the Laptev Sea shelf (see section 4.1 and Figure 7) both the DFe concentrations and river water fractions increased again.

[24] Toward the Amundsen Basin an increase was observed in the DFe concentrations that coincides with high river water fractions (>10%) and sea-ice formation (negative sea-ice meltwater fraction) (Figure 5; see section at ~600–100 km and at ~2500 km). This pattern was observed somewhat more pronounced, in the Makarov Basin further west (Figure 5; see section at ~1100–1500 km and 2000–2400 km). A considerable influence of Pacific water (>20%) was observed in the entire Makarov Basin. On the North American side of the Transpolar Drift, Pacific-derived waters comprised a major fraction of the upper water column seen most pronounced at station 342 with $f_p \sim 90\%$ (Figure 5). The maximum in Pacific fractions coincides with a strong DFe minimum, observed for all stations on the North American side of the TPD.

5. Discussion

[25] The inverse linear relationship between DFe and salinity (Figure 8a) demonstrates the important role of Arctic rivers in the delivery of DFe to the Arctic Ocean. Nevertheless, significant deviations from the linear trend indicate that there are also other important sources and processes. In the following discussion we first compare our results with existing (D)Fe data from the Arctic (section 5.1) and discuss the processes on the shelf seas (section 5.2). Then we discuss the concentration of DFe in freshwater sources (section 5.3) and compare the distribution of DFe in the central Arctic Ocean with the distribution of freshwater (section 5.4). Processes involved in sea-ice formation and transport will alter the ratio of total Fe (TFe) and the dissolved fraction (DFe). Therefore, in order to understand the impact of these sea-ice processes on the Fe distribution the ratio TFe/DFe is discussed (section 5.5).

5.1. Comparison With Previously Published Data

[26] Our study shows that concentrations of DFe in Siberian shelf seas are relatively low (<1 nM), except for the Laptev Sea where rather high concentrations (>10 nM) are observed. In the central Arctic, concentrations vary from ~0.5 nM in the Nansen Basin, to >2 nM in the Amundsen and Makarov basins. To our knowledge no other data has been previously reported for dissolved (0.2 μm filtered) DFe in the Arctic Ocean, but there are some studies reporting unfiltered Fe concentrations. Our observations are consistent with data of *Moore* [1983], who reported a profile with ~1.5 nM of reactive iron in the surface waters above the Lomonosov Ridge. *Measures* [1999] reported generally higher concentrations in the range of 0.67–20 nM for reactive Fe on a transect across the Arctic Ocean, with 1.55–3.5 nM over the Lomonosov Ridge and the Makarov Basin and 0.67–1.31 nM for the western Nansen Basin. These ranges of unfiltered samples are slightly higher than the data presented here for filtered samples, but agree well with the values for unfiltered samples from our same casts [*Thuroczy et al.*, 2011]. *Tovar-Sanchez et al.* [2009] reported Fe concentrations of 10 ± 1.8 nM (n = 10) in upper surface waters (1 m depth) just north of Spitsbergen and values are thereby

roughly an order of magnitude higher than our data sampled slightly to the east at ~15–20° (see Figures 2 and 3). However, the difference may be at least partly explained by the fact that *Tovar-Sanchez et al.* [2009] reported unfiltered Fe and sampled at ~1 m water depth to specifically capture the influence of melting of sea-ice. In contrast filtered (dissolved) Fe concentrations reported here are from >10 m water depth.

5.2. Shelf Seas

[27] In the Barents Sea, all stations show a subsurface DFe minimum, often coinciding with a maximum in fluorescence (Figure 2a). This fluorescence is due to presence of chl a, and may indicate uptake of DFe by phytoplankton. *Cai et al.* [2010] report a relatively high POC export in the Barents Sea from measurements collected on the same expedition, indicating significant primary production in the months before the expedition. Indeed, NASA Sea-viewing Wide Field-of-view Sensor (SeaWiFS) images show high concentrations of chlorophyll (~5 mg m^{-3}) in the Barents Sea in the months before our cruise (May–June) [*Feldman and McClain*, 2011]. During our expedition concentrations had already decreased to (<1 mg m^{-3}) (NASA SeaWiFS images [*Feldman and McClain*, 2011]) (Figures S1a–S1d). Moreover, the chl a distribution in the Barents Sea shows variations of one order of magnitude in the region southeast of Spitsbergen in June–July 2007. Also satellite derived annual primary production data of the calendar year 2007 from the Arctic Ocean, show variations between 50 and 150 g C m^{-2} yr^{-1} over the Barents Sea Shelf [*Arrigo et al.*, 2008]. Therefore, it is likely that biological uptake and depletion of DFe in the months prior to the expedition has led to the observed low concentrations. Of the four Barents Sea stations, station 237 has the lowest POC export [*Cai et al.*, 2010] and relatively higher DFe, suggesting little DFe depletion by phytoplankton at this station, consistent with spatial variation within the Barents Sea (Figure 3). The very high DFe concentration (~1.67 nM) close to bottom depth at station 236 is consistent with a similar high concentration observed in DMn distribution and is attributed to benthic efflux [*Middag et al.*, 2011]. The Kara Sea stations differ from the Barents Sea and Laptev Sea shelf sea stations as they are situated all on the outer shelf, close to the slope, rather than on the central shelf (Figure 1b, enlargement). All Kara Sea stations show an upper surface biological depletion in DFe, consistent with the maximum chl a fluorescence signal in the upper 20 m surface water (Figure 2b). Station 271, situated furthest from the shelf, shows a small intrusion of cold, fresher, slightly less oxygenated waters (Figure 2b), likely from the shelf, below a stable mixed layer (upper 15 m). Higher DFe in these advected shelf waters may explain the higher DFe in the upper 25 m at station 271. Similarly, an even stronger decrease in salinity and oxygen may indicate intruding waters from the shelf at station 279, and thus explain the high DFe concentrations, although this is not confirmed in the θ profile (Figure 2b). Below the upper 50 m the Atlantic core is recognized by higher θ and salinity; at station 271 and station 279 at ~75 to 175 m water depth. At stations, 272 and 276, situated further from the shelf, a deeper Atlantic water layer is observed. Below 100 m, the slightly lower DFe at station 271 and 272 (~0.4–0.45 nM) may be due to influence of Fram Strait Branch Waters, whereas the DFe at station 276 and 279 (~0.5–0.55 nM) may be influenced by Barents Sea Branch Waters (Figure 4). In general, the DFe concentrations are slightly lower in the Kara Sea than in the Barents Sea; DFe may be removed during transport from the Atlantic source to the Kara Sea both by adsorptive scavenging removal and/or biological uptake. Remarkably, the profile of dissolved Barium (Ba) as measured at station 276 follows a reverse pattern as DFe at this depth, with a small decrease at ~100–125 m (Roeske et al., submitted manuscript, 2011, Figure 4). It may be possible that some small influence of advected shelf waters with a (small) sea-ice meltwater signal at ~100–125 m depth causes the lower Ba (Roeske et al., submitted manuscript, 2011) yet higher DFe concentrations. Although these data do not provide a definitive conclusion, our suggestion of advected water with elevated sea-ice meltwater influence is consistent with the deviations observed in the salinity profile (Figure 2b), high dissolved Al at a depth of 125 m [*Middag et al.*, 2009] and the higher $\delta^{18}O$ (not shown) at these depths. The DFe concentrations gradually decrease at Station 276 below 300 m to ~0.45 nM at 620 m depth.

[28] In the Laptev Sea (station 411; see Figure 7) a very low light transmission signal is found below 20 m, corresponding to extremely high DFe. Because low light transmission indicates presence of particles, local resuspension from bottom sediment may be an input source for DFe (Figure 2c). Moreover, these enhanced DFe concentrations in the bottom waters may come from the rapid regeneration at depth of organic material exported from the upper waters. This mechanism has been reported for dissolved Barium (Ba) that shows a similar distribution with high concentrations in Laptev Sea bottom waters [*Abrahamsen et al.*, 2009; Roeske et al., submitted manuscript, 2011]. Organic matter in this part of the Laptev Sea is mainly of terrestrial origin [*Anderson et al.*, 2009]; the dissolution of this organic matter may explain the observed high concentrations of DFe. Additionally, bottom waters on the Laptev Sea shelf are known to contain some river water and are also influenced by sea-ice formation (Figure 7) [*Bauch et al.*, 2009]. Since river water fractions do not differ as much between surface and bottom layer (Figure 7) the extremely enhanced DFe concentrations in the bottom layer are not primarily determined by river contribution. Brine rejection from sea-ice formation may be of importance in distributing DFe over the water column. For the Weddell Sea, *Lannuzel et al.* [2008] reported DFe enrichment upon brine drainage. Close to the shelf edge, the station 407 shows relatively lower DFe and higher salinity, than station 411 on the shelf (Figure 2c), due to the Atlantic Boundary Current flowing along the Arctic shelf seas [*Rudels et al.*, 2004] transporting saline water with relatively low DFe (Klunder et al., submitted manuscript, 2011) onto the outer Laptev Sea shelf.

5.3. Fe in Freshwater Sources

[29] The inflow of river water is a major source of DFe to surface waters. The DFe concentrations in Arctic rivers vary considerably. *Dai and Martin* [1995] reported 250–650 nM for the Ob and Yenisey rivers and *Hölemann et al.* [2005] reported a range of 410–7132 nM for the Lena River. Concentrations of DFe in river water are seasonally variable: both the North American and Eurasian rivers show a strong seasonal summer peak in their discharge volume with higher DFe concentration during the peak discharge [*Rember and*

Trefry, 2004; *Hölemann et al.*, 2005]. These concentrations are orders of magnitude higher than common ocean seawater concentrations, however, a large amount of DFe is expected to be removed by precipitation/flocculation and sinking in the estuaries [*Boyle et al.*, 1977].

[30] The melting of seasonal sea-ice is another possible input source of DFe [*Measures*, 1999]. In the Southern Ocean, melting of seasonal sea-ice has been shown to cause enrichment of DFe [*Klunder et al.*, 2011; *Lannuzel et al.*, 2008]. It is important to note that the DFe concentration in sea-ice can be modified by biological processes (uptake by phytoplankton and bacterial remineralization) [*van der Merwe et al.*, 2009]. Also Arctic sea-ice may receive Fe from atmospheric sources [*Darby et al.*, 1974]. However, because the Arctic sea-ice is largely formed on the Arctic shelves, the entrainment of sediments, either from rivers or suspension at the shelf can be assumed to be a more significant process [*Nürnberg et al.*, 1994]. *Hölemann et al.* [2005] reported very high (281–10585 nM) DFe concentrations in sea-ice in the Laptev Sea, where the concentrations near the Lena River Delta exceeded the concentrations further on the shelf by two orders of magnitude. *Tovar-Sanchez et al.* [2009] reported concentrations of 532–864 nM total dissolvable Fe in Arctic sea-ice for stations north of Spitsbergen. This wide range of Fe enrichment in samples taken relatively close to each other illustrates the strong spatial variability of the input of sea-ice derived particulate and dissolved Fe, that will lead to patchiness in the distribution of DFe in Arctic sea-ice meltwater and consequently in the water below.

[31] Moreover, the contribution of dissolved Fe to the total Fe in sea-ice cores has been shown to vary between less than 1% and 33% in the Subarctic Bering Sea [*Aguilar-Islas et al.*, 2008]. This stresses the role of release mechanisms and dissolution processes in delivery of dissolved Fe from sea ice sediments to the water column [*Cámara-Mor et al.*, 2010; *Nürnberg et al.*, 1994]. The Transpolar Drift (TPD) carries sediment laden sea-ice to the central Arctic where it can be released upon melting [*Cámara-Mor et al.*, 2010; *Nürnberg et al.*, 1994]. It is important to note that the mass balance equations used in this study yield a net value of the sea-ice contribution over the residence time of the water and melting as well as formation may have taken place before the time of measurement. Therefore water with a negative value for the fraction sea-ice meltwater (reflecting net sea-ice formation) may still contain some recent addition of sea-ice meltwater, i.e., may still have a sea-ice related DFe source.

[32] In the Makarov Basin, a large part of the freshwater component is due to waters of Pacific origin. This water may contain a different DFe signature compared to the marine waters in the Eurasian Basin that consist primarily of Atlantic-derived waters [*Bauch et al.*, 2011]. The DFe concentrations in the surface waters of the North Pacific vary widely (0.1–3 nM) [*Takata et al.*, 2004; *Moore and Braucher*, 2008; *Aguilar-Islas et al.*, 2008]. Besides this wide range in concentration of DFe in the North Pacific Ocean, there is significant biogeochemical modification of Pacific waters during transit over the shallow shelves from the Bering Sea to the central Arctic [*Codispoti et al.*, 2005] (transit time in the order of 1–6 months [*Woodgate et al.*, 2005]). Therefore, the DFe end-member concentration in Pacific-derived waters in the Arctic Ocean halocline has a wide range and cannot be defined as one single end-member value.

5.4. DFe Concentration in Correlation to Freshwater Distribution

[33] The strong linear relationship between DFe and river water in the surface layer of the central Arctic (Figure 8b) indicates that river water is the most important DFe source in the central Arctic Ocean. The DFe concentration does not exceed 1.5 nM in regions with river water fractions <10%, whereas in regions with >15% river water fraction, DFe concentrations of up to 3 nM are found.

[34] The small portion of total freshwater (river water and sea-ice meltwater < ~6%) present in the Eastern Nansen Basin and over the Barents Sea and Kara Sea shelves does not show a clear correlation with the distribution of DFe. Sea-ice meltwater contributes about half of this freshwater but no related increase in DFe is observed (Figures 3 and 4). Thus sea-ice meltwater is generally not a significant source of DFe in this region. At the northernmost station of transect 1 (Figure 3) and east of the St. Anna Trough (Figure 4) small but significant input of river water correlated with high DFe. This river water originates from shelf regions further east where it becomes frozen and next transported as ice together with sea-ice [*Bauch et al.*, 2011], and it melts again in the Barents Sea and eastern Nansen Basin. The DFe present in this river water transported as ice may be subject to biological Fe-depletion during transport causing strong spatial variation in concentrations of DFe (see section 5.3). Also, both the strong surface depletion in phosphate (Figure S2) and the relatively high POC-export fluxes (1.7–5.5 mmol m^{-2} d^{-1}) [*Cai et al.*, 2010] indicate phytoplankton growth and subsequent export in the months prior to our expedition (see section 5.2). If this production would take up the DFe from sea-ice meltwater it would not be observed in the DFe concentrations despite considerable river water and sea-ice meltwater fractions. The facts that melting of sea-ice in the Barents Sea commenced in mid-May 2007 [*Spreen and Kaleschke*, 2008] and our sampling in the Barents Sea took place at the end of July 2007 are in favor of such a mechanism, which was also observed in the Ross Sea [*Sedwick and DiTullio*, 1997].

[35] The two stations at the North American side of the TPD (station 338 and 342, Figure 1a) significantly deviate from the correlation between DFe and river water fractions seen in the Eurasian Basin and in the TPD (Figure 9). While river water fractions are lower compared to values found in the TPD, still significant river water fractions are observed which are not reflected in the actually low DFe concentrations (Figure 5). At stations 338 and 342 an enrichment of DFe is observed at the surface, lower DFe concentration at the subsurface and another DFe-enrichment at 75–100 m depth (Figure 9). Salinity at these stations is low at the surface, but increases in the upper 30 m, remains relatively constant between ~30–60 m depth and continues to increase below (Figure 9). Compared to salinity values found at ~60 m an additional input of 1–2% freshwater (S = 0) is needed to obtain the low salinity values found in the upper 30 m. Moreover, there is a DFe decrease of 0.32 nM from 10 to 50 m and of 0.15 nM from 10 to 25 m for station 338 and 342 respectively. Although the fraction of (Eurasian) river water is high compared to that of sea-ice meltwater (8–10%), the river water fractions are relatively constant over the upper 50 m, whereas positive sea-ice-meltwater fractions (~3%)

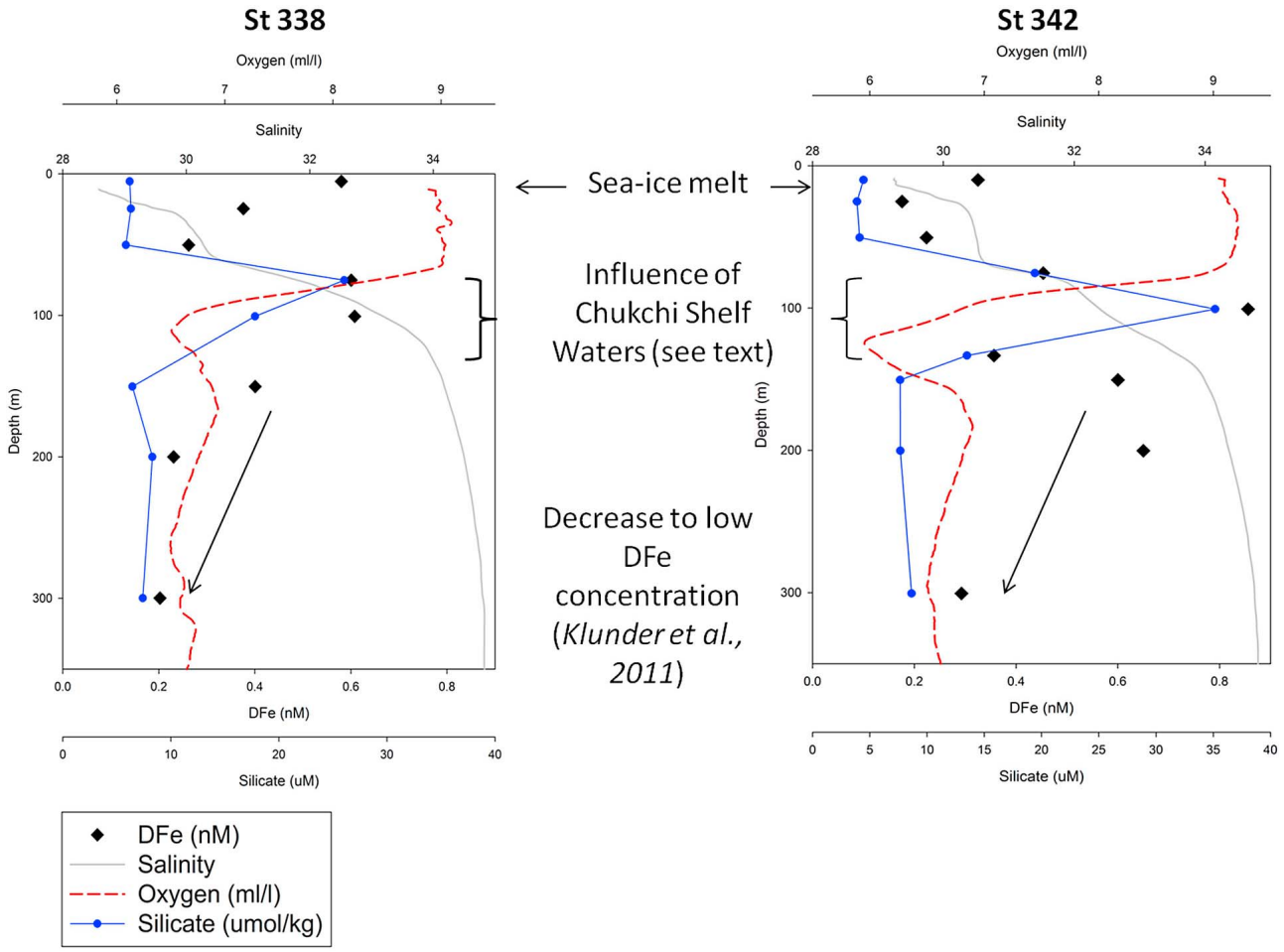

Figure 9. Depth profiles in upper 300 m of DFe (nM), oxygen, salinity and salinity for stations (left) 338 and (right) 342 located on the North American side of the Transpolar Drift. Processes influencing the concentration of DFe are indicated (see text for explanation).

are only observed in the shallowest sample (~10 m) and are consistent with the high DFe concentrations. From the lower salinity in the upper ~10 m, relative to the winter mixed layer salinity and the observed relation of high DFe with sea-ice meltwater it is suggested that the low salinity, high DFe input comes from the surface. Assuming DFe enrichment is caused solely by sea ice meltwater, the DFe end-member concentration is calculated using the extra sea-ice meltwater input of 2% and 1.5% and the DFe decrease of 0.32 and 0.15 nM respectively. The DFe-concentration for the sea-ice meltwater end-member should thereby be ~16 nM and ~10 nM DFe, for stations 338 and 342 respectively. This calculated DFe concentration for the sea-ice end-member is low compared to the reported DFe in Arctic sea-ice (see section 5.3). However, we may expect strong spatial variations in the amount of DFe released from melting of sediment laden sea-ice as it is dependent on the amount of sediment contained in the ice and on the dissolution mechanisms. The presence of chlorophyll a in the upper 50 m [*Cai et al.*, 2010], may point to biological depletion causing the lower DFe concentrations at ~25–50 m depth. Instead of North American river water, Roeske et al. (submitted manuscript, 2011) attributed the waters at 50–100 m depth to halocline waters from the Chukchi Shelf, carrying the properties of mineralization processes between bottom waters and sediment. This is reflected in high Ba concentrations (Roeske et al., submitted manuscript, 2011) and low O_2 and high silicate concentrations (Figure 9). These mineralization processes could cause the DFe increase from 50 m to ~100 m at station 338 and 342. The strongest influence of these waters from the Chukchi Sea is found at 100 m depth at station 342 as reflected in the Si maximum (Figure 9) and may explain the high DFe concentrations here. In contrast, lower DFe concentrations (Figure 9) at station 338 may be caused by mixing with Atlantic waters, which comprise already >60% of the water mass at 100 m. Below ~125 m, the DFe decreases (Figure 9), consistent with the DFe concentration observed in the deep waters of the Makarov Basin (Klunder et al., submitted manuscript, 2011).

[36] An alternative explanation for the relatively low DFe values on the North American side of the TPD is the longer transit time of waters from the shelf seas to the central Arctic in the Beaufort Gyre compared to the fast transport of river derived waters from the shelf to the central Arctic by the TPD. This longer transit time would allow more Fe to be removed by scavenging processes. In addition, DFe may be taken up by phytoplankton in the preceding months, enhanced by the largely ice-free conditions in 2007 in this part of the Canadian Basin [*Arrigo et al.*, 2008].

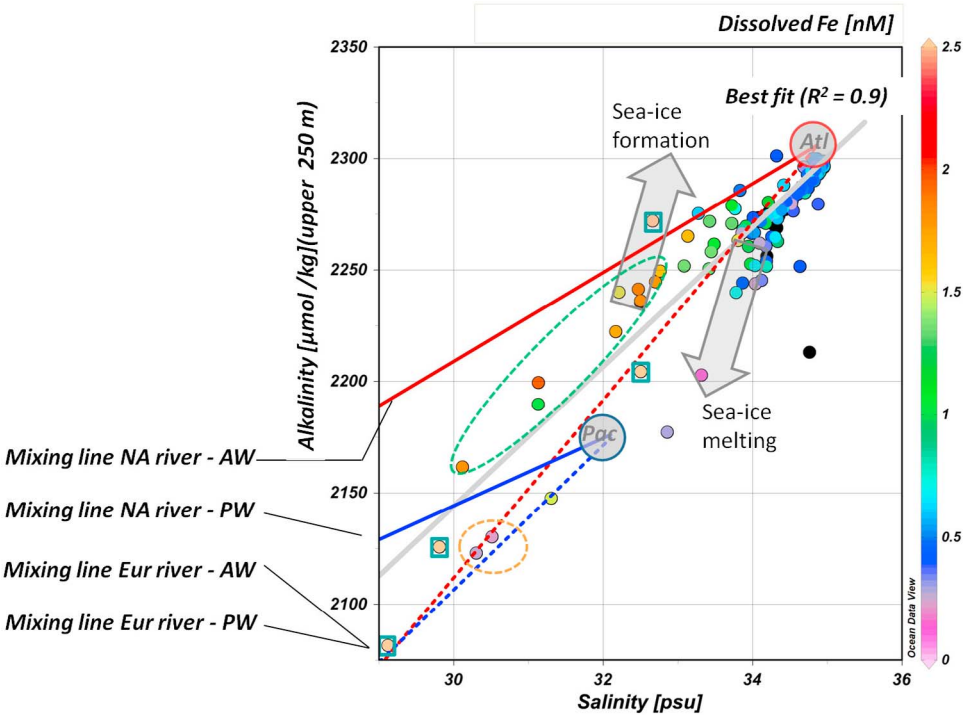

Figure 10. Relation between total alkalinity and salinity for the stations in the upper 250 m. DFe concentrations are shown in color. Mixing lines between Atlantic water and Eurasian (red dotted) and North American river water (red solid) and Pacific water and Eurasian (blue dotted) and North American river water (blue solid). End-member concentrations are following *Yamamoto-Kawai et al.* [2005]. Salinity for Atlantic water is 34.87 and for Pacific water is 32.2 (mean of 32.7 [*Ekwurzel et al.*, 2001] and 31.5 [*Anderson et al.*, 1994]). Total alkalinity for Atlantic water is 2306 μmol/kg and for Pacific water is 2173 μmol/kg [*Anderson et al.*, 1994]. The river end-members are calculated using Sal = 0 and alkalinity values of 1181, 845, 788, 1707 and 1540 μmol/kg for the Ob, Yenisey, Lena, Yukon and Mackenzie rivers, respectively [*Cooper et al.*, 2008], multiplied with the partial distribution of these rivers to the total end-member [*Holmes et al.*, 2002]. Gray arrows indicate sea-ice melting and sea-ice formation, relative to the Atlantic-Eurasian river water mixing line. Green ellipse includes the data points at ~50 m in the TPD (stations 309–333 and 349–352) and orange ellipse indicates the waters at ~50 m north of the TPD. Laptev Sea data points (stations 407 and 411) are surrounded by a blue square and are consistent with mixing with river water and a strong sea-ice formation/brine input signal in the deepest layer of station 411 (see text section 5.2).

[37] A small subset of stations were also sampled for total alkalinity (A_T). The A_T data supports the finding that the low salinity (and high DFe input) within the TPD is caused by (mixing with) Eurasian river water, whereas the stations on the North American side of the TPD have a different freshwater signature. In Figure 10 the A_T versus salinity relationship is depicted, including the mixing lines between Atlantic, Pacific, North American river water and Eurasian river water end-members (see caption for end-member values). The DFe concentrations are shown in color. The high A_T, high salinity waters with low/moderate DFe, are mainly Nansen Basin waters. As aforementioned, some stations in this region are influenced by sea-ice meltwater (following gray arrow, Figure 10). A decrease in A_T and salinity is seen at ~50 m (shallowest sampling depth for A_T) in the stations within the TPD (green ellipse), where also DFe concentrations increase. Remarkably, these data points lie between the Atlantic water/Eurasian river water and Atlantic water/North American river water mixing lines. Substantial ice formation, as has been observed in the TPD (Figure 5), would result in the observed deviation from the Atlantic water/Eurasian river water mixing line. Nevertheless, influence of North American rivers to the TPD cannot be ruled out. There are two data points at ~50 m depth on the North American side of the TPD, showing a lower A_T relative to their salinity than within the TPD (orange ellipse). These data points are on the mixing line of Eurasian river water and Pacific water (Figure 10). This is consistent with the observed river water fractions of ~6–8 (Figure 5) and influence of Pacific water flowing over the Chukchi Shelf (see section 5.3) (see also Roeske et al., submitted manuscript, 2011). *Anderson et al.* [2004] noted that biological processes little affect the A_T in the Arctic Ocean which is in line with little change observed in A_T concentrations during transit over the Chukchi shelf.

5.5. Dissolved Versus Total Dissolvable Fe: Implications for Fe Delivery to the Arctic

[38] Recent melt of sediment laden sea-ice or influx of riverine sediments from the shelves would result in a high

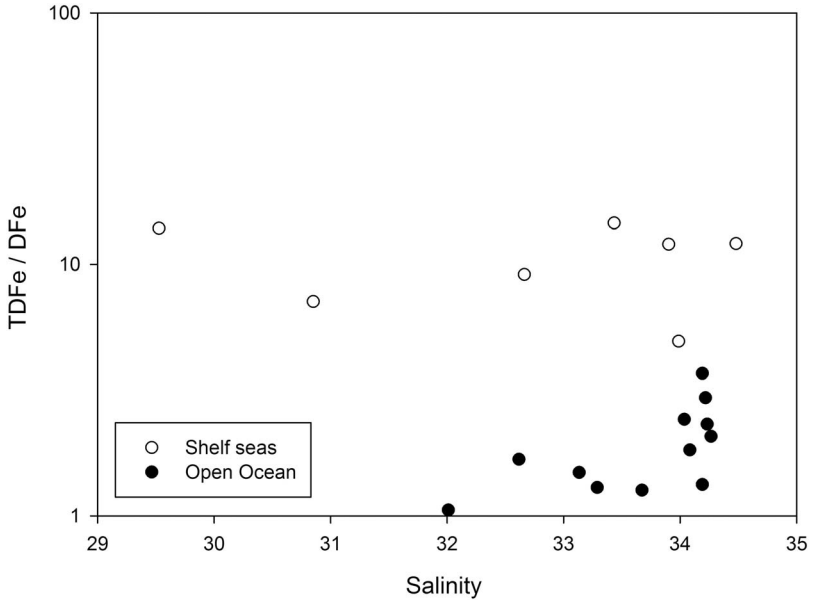

Figure 11. Ratio total iron (TFe) over dissolved iron (DFe) for all points in the upper 100 m at shelf stations (open circles) and open ocean stations (solid circles). Shelf sea stations are indicated in Figure 1b.

concentration of Fe in the particulate phase and thus a relatively high unfiltered (total dissolvable) Fe concentration (TDFe). During transit from the shelves to the central Arctic, dissolution processes, sinking and particle scavenging will lower the ratio of TDFe relative to DFe. Thus the ratio TDFe/DFe may give insight in these processes. For instance a rapid removal of TDFe compared to DFe with offshore distance from the Antarctic Peninsula was observed [*Ardelan et al.*, 2010] indicating strong settling loss of TDFe relative to DFe in surface waters. Figure 11 shows the TDFe/DFe ratios versus salinity in the upper 100 m for stations on the Siberian shelves and for open ocean stations. Generally, the TDFe/DFe ratios are lower for open ocean stations than for shelf stations (closed and open dots in Figure 11, respectively). The higher ratio at shelf stations indicates a strong and recent input of sediments, released during local melting of sea-ice or from rivers and causing very high Fe concentrations in the size fraction >0.2 μm. We suggest that recent local sea-ice meltwater was not present in the central Arctic Ocean and that during transit from the shelf seas to the central Arctic Ocean most of the Fe in the particulate fraction is removed, resulting in TDFe/DFe ratios close to 1 at these stations (Figure 11). In sea-ice cores from the Bering Sea the TDFe/TFe ratio is between 2.6 and 1800 (median 42) [*Aguilar-Islas et al.*, 2008], close to the TDFe/DFe ratios observed for shelf stations rather than to those observed in the central Arctic (Figure 11). This strengthens our concept that river water rather than meltwater of sediment laden sea-ice is the dominant DFe input source in the central Arctic Ocean. In principle the melting of possibly sediment laden sea-ice at stations 338 and 342 should be visible in high TDFe/DFe ratios. Unfortunately this remains speculative because no TDFe measurements are available from stations 338 and 342.

6. Summary and Conclusion

[39] The data reveal that the DFe distribution throughout the surface waters of the central Arctic Ocean is largely correlated with freshwater input sources, which is predominantly Eurasian river water. On the shelves other factors influence the Fe distribution. In the Barents Sea and Kara Sea, DFe minima at high chl a concentrations indicate DFe depletion by phytoplankton growth. Strong carbon export and high chlorophyll abundance from satellite images indicate that it is likely that DFe input enabled primary production in the months prior to our cruise. This input likely comes from sea-ice meltwater and ice transported river water in the Barents Sea. Biological depletion of DFe could then explain the relatively low DFe concentrations despite significant sea-ice meltwater and river water signals. Very high DFe concentrations near the bottom of the Laptev Sea are attributed to either sediment resuspension, sinking of brine, or regeneration of Fe in the bottom layer.

[40] In the central Arctic, both the Atlantic boundary current and the Transpolar Drift transport DFe within Arctic surface waters. The DFe concentration in the western part of the Eurasian Basin reflects mainly the concentrations of Atlantic surface water. The influence of Atlantic water can still be recognized at the Laptev Sea continental margin, in high salinities and relatively low DFe. Freshwater from the Eurasian rivers mainly transported by the TPD is the main contributor to DFe in the Amundsen and Makarov basins, where DFe concentrations >2 nM are observed. Here, the ratios of dissolved relative to "total dissolvable" Fe are low, likely due to dissolution of DFe and scavenging/sinking of DFe in the "total dissolvable" fraction. Above the Mendeleev-Alpha Ridge, on the North American side of the Transpolar Drift, two stations deviate from the pattern of river transported DFe. Here the DFe concentrations are generally lower than those within surface layer water of the TPD. This may be caused by the presence of Pacific-derived waters having lower DFe concentrations due to biological depletion during transit, but also by (Eurasian) river water with longer residence times compared to river water in the Eurasian Basin and the TPD. Scavenging and uptake by

phytoplankton during transport from the shelves may lower DFe concentrations. Mixing of river water with Atlantic- and Pacific-derived waters within the TPD and on the North American side of the TPD, respectively is also observed from the distribution of Total Alkalinity. More specifically, the DFe concentrations on the North American side of the Transpolar Drift are strongly determined by sea-ice meltwater in the upper 50 m. A significant influence of remineralization is seen DFe enrichment at ~100 m depth, However, generally biological depletion of these waters during transit over the shelves results in a overall low DFe concentration.

[41] The results suggest that shifts in delivery of DFe to the Arctic Ocean with regard to the regional change in climate may primarily depend on shifts in Arctic currents (e.g., shift in the position of the TPD) and on the amount of river runoff rather than on an expected further increase in sea-ice meltwater. However, loss of Arctic sea-ice cover also alters an important transport mechanism of river derived DFe within the Arctic Ocean and specially the Arctic shelf seas, which are the most productive areas [*Pabi et al.*, 2008]. Recently *Arrigo et al.* [2008] suggested an increase in denitrification in the Arctic Ocean, resulting in a further depletion of the already low nitrogen concentrations in the waters leaving the Arctic to the North Atlantic, this likely enhancing N_2 fixation in the North Atlantic [*Arrigo et al.*, 2008; *Yamamoto-Kawai et al.*, 2006]. This raises the question whether the Fe concentrations in the waters transported from the Arctic to the North Atlantic would contain enough Fe, which is reported to be a control factor for N_2 fixation [*Falkowski et al.*, 1998], to sustain such enhanced N_2-fixation. Based on the results of this study, we may carefully confirm the relatively high concentration of DFe in the waters exiting the Arctic relative to the lower DFe in common North Atlantic surface waters [*Moore and Braucher*, 2008].

[42] **Acknowledgments.** The authors want to thank captain S. Schwarze and his crew of FS Polarstern for excellent support throughout the expedition. Lorendz Boom is gratefully acknowledged for operating the ultraclean sampling system. Karel Bakker is gratefully thanked for accurate measurements of the major nutrients. Charles-Edouard Thuroczy is acknowledged as one of our ultraclean subsampling and filtration team. The authors thank two anonymous reviewers for their constructive comments. The Netherlands GEOTRACES program in the International Polar Year (2007–2008) was supported by the Netherlands Organization for Scientific Research (Nederlandse Organisatie voor Wetenschappelijk Onderzoek, NWO); D.B. was funded under grant SP526/3 by the German Research Foundation (DFG).

References

Aagaard, K., and E. C. Carmack (1989), The role of sea ice and other freshwater in the Arctic circulation, *J. Geophys. Res.*, *94*(C10), 14,485–14,498, doi:10.1029/JC094iC10p14485.

Aagaard, K., L. K. Coachman, and E. Carmack (1981), On the halocline of the Arctic Ocean, *Deep Sea Res. Part A*, *28*(6), 529–545, doi:10.1016/0198-0149(81)90115-1.

Abrahamsen, E. P., et al. (2009), Tracer $\delta^{18}O$ derived freshwater composition of the Siberian continental shelf and slope following the extreme Arctic summer of 2007, *Geophys. Res. Lett.*, *36*, L07602, doi:10.1029/2009GL037341.

Aguilar-Islas, A. M., R. D. Rember, C. W. Mordy, and J. Wu (2008), Sea ice-derived dissolved iron and its potential influence on the spring algal bloom in the Bering Sea, *Geophys. Res. Lett.*, *35*, L24601, doi:10.1029/2008GL035736.

Anderson, L., G. Björk, O. Holby, E. Jones, G. Kattner, K. Koltermann, B. Liljeblad, R. Lindegren, B. Rudels, and J. Swift (1994), Water masses and circulation in the Eurasian Basin: Results from the *Oden* 91 expedition, *J. Geophys. Res.*, *99*, 3273–3283, doi:10.1029/93JC02977.

Anderson, L. G., S. Jutterström, S. Kaltin, E. P. Jones, and G. Björk (2004), Variability in river runoff distribution in the Eurasian Basin of the Arctic Ocean, *J. Geophys. Res.*, *109*, C01016, doi:10.1029/2003JC001773.

Anderson, L. G., S. Jutterström, S. Hjalmarsson, I. Wåhlström, and I. P. Semiletov (2009), Out-gassing of CO_2 from Siberian Shelf seas by terrestrial organic matter decomposition, *Geophys. Res. Lett.*, *36*, L20601, doi:10.1029/2009GL040046.

Ardelan, M. V., O. Holm-Hansen, C. D. Hewes, C. S. Reiss, N. S. Silva, H. Dulaiova, E. Steinnes, and E. Sakshaug (2010), Natural iron enrichment around the Antarctic Peninsula in the Southern Ocean, *Biogeosciences*, *7*(1), 11–25, doi:10.5194/bg-7-11-2010.

Arrigo, K. R., G. van Dijken, and S. Pabi (2008), Impact of a shrinking Arctic ice cover on marine primary production, *Geophys. Res. Lett.*, *35*, L19603, doi:10.1029/2008GL035028.

Bauch, D., P. Schlosser, and R. G. Fairbanks (1995), Freshwater balance and the sources of deep and bottom waters in the Arctic Ocean inferred from the distribution of $H_2^{18}O$, *Prog. Oceanogr.*, *35*(1), 53–80, doi:10.1016/0079-6611(95)00005-2.

Bauch, D., I. A. Dmitrenko, C. Wegner, J. Hölemann, S. A. Kirillov, L. A. Timokhov, and H. Kassens (2009), Exchange of Laptev Sea and Arctic Ocean halocline waters in response to atmospheric forcing, *J. Geophys. Res.*, *114*, C05008, doi:10.1029/2008JC005062.

Bauch, D., M. Rutgers van der Loeff, N. Andersen, S. Torres-Valdes, K. Bakker, and E. P. Abrahamsen (2011), Origin of freshwater and polynya water in the Arctic Ocean halocline in summer 2007, *Prog. Oceanogr.*, *91*, 482–495, doi:10.1016/j.pocean.2011.07.017.

Boyd, P., A. Watson, C. Law, E. Abraham, T. Trull, R. Murdoch, D. Bakker, A. Bowie, K. Buesseler, and H. Chang (2000), A mesoscale phytoplankton bloom in the polar Southern Ocean stimulated by iron fertilization, *Nature*, *407*(6805), 695–702, doi:10.1038/35037500.

Boyle, E. A., J. M. Edmund, and E. R. Sholkovitz (1977), The mechanism of iron removal in estuaries, *Geochim. Cosmochim. Acta*, *41*(9), 1313–1324, doi:10.1016/0016-7037(77)90075-8.

Broecker, W. S., T. Takahashi, and T. Takahashi (1985), Sources and flow patterns of deep-ocean waters as deduced from potential temperature, salinity, and initial phosphate concentration, *J. Geophys. Res.*, *90*(C4), 6925–6939, doi:10.1029/JC090iC04p06925.

Cai, P., M. Rutgers van der Loeff, I. Stimac, E. M. Nöthig, K. Lepore, and S. B. Moran (2010), Low export flux of particulate organic carbon in the central Arctic Ocean as revealed by ^{234}Th:^{238}U disequilibrium, *J. Geophys. Res.*, *115*, C10037, doi:10.1029/2009JC005595.

Cámara-Mor, P., P. Masqué, J. Garcia-Orellana, J. K. Cochran, J. L. Mas, E. Chamizo, and C. Hanfland (2010), Arctic Ocean sea ice drift origin derived from artificial radionuclides, *Sci. Total Environ.*, *408*(16), 3349–3358, doi:10.1016/j.scitotenv.2010.03.041.

Carmack, E., and P. Wassmann (2006), Food webs and physical-biological coupling on pan-Arctic shelves: Unifying concepts and comprehensive perspectives, *Prog. Oceanogr.*, *71*(2–4), 446–477, doi:10.1016/j.pocean.2006.10.004.

Codispoti, L. A., C. Flagg, V. Kelly, and J. H. Swift (2005), Hydrographic conditions during the 2002 SBI process experiments, *Deep Sea Res. Part II*, *52*(24–26), 3199–3226, doi:10.1016/j.dsr2.2005.10.007.

Cooper, L. W., J. W. McCelland, R. M. Holmes, P. A. Raymond, J. J. Gibson, C. K. Guay, and B. J. Peterson (2008), Flow-weighted values of runoff tracers ($\delta^{18}O$, DOC, Ba, alkalinity) from the six largest Arctic rivers, *Geophys. Res. Lett.*, *35*, L18606, doi:10.1029/2008GL035007.

Craig, H. (1961), Isotopic variations in meteoric waters, *Science*, *133*, 1702–1703, doi:10.1126/science.133.3465.1702.

Dai, M.-H., and J.-M. Martin (1995), First data on trace metal level and behaviour in two major Arctic river-estuarine systems (Ob and Yenisey) and in the adjacent Kara Sea, Russia, *Earth Planet. Sci. Lett.*, *131*(3–4), 127–141, doi:10.1016/0012-821X(95)00021-4.

Darby, D. A., L. H. Burckle, and D. L. Clark (1974), Airborne dust on the Arctic pack ice, its composition and fallout rate, *Earth Planet. Sci. Lett.*, *24*(2), 166–172, doi:10.1016/0012-821X(74)90093-4.

de Baar, H. J. W., J. T. M. de Jong, D. C. E. Bakker, B. M. Loscher, C. Veth, U. Bathmann, and V. Smetacek (1995), Importance of iron for plankton blooms and carbon dioxide drawdown in the Southern Ocean, *Nature*, *373*(6513), 412–415, doi:10.1038/373412a0.

de Baar, H. J. W., et al. (2008), Titan: A new facility for ultraclean sampling of trace elements and isotopes in the international Geotraces program, *Mar. Chem.*, *111*(1–2), 4–21, doi:10.1016/j.marchem.2007.07.009.

Dickson, A. (2001), Reference material for oceanic CO_2 measurements, *Oceanography*, *14*, 21–22.

Dickson, A. G., C. L. Sabine, and J. Christian (2007), *Guide to Best Practices for Ocean CO_2 Measurements*, *PICES Spec. Publ. Ser.*, vol. 3, 191 pp., Oak Ridge Natl. Lab., Oak Ridge, Tenn.

Ekwurzel, B., P. Schlosser, R. A. Mortlock, R. G. Fairbanks, and J. H. Swift (2001), River runoff, sea-ice meltwater, and Pacific water distribution and

mean residence times in the Arctic Ocean, *J. Geophys. Res.*, *106*(C5), 9075–9092, doi:10.1029/1999JC000024.

Falkowski, P. G., R. T. Barber, and V. Smetacek (1998), Biogeochemical controls and feedbacks in ocean primary production, *Science*, *281*, 200–206.

Feldman, G. C., and C. R. McClain (2011), OceanColor Web, http://oceancolor.gsfc.nasa.gov/, NASA Goddard Space Flight Cent., Greenbelt, Md.

Gebhardt, A. C., F. Schoster, B. Gaye-Haake, B. Beeskow, V. Rachold, D. Unger, and V. Ittekkot (2005), The turbidity maximum zone of the Yenisei River (Siberia) and its impact on organic and inorganic proxies, *Estuarine Coastal Shelf Sci.*, *65*(1–2), 61–73, doi:10.1016/j.ecss.2005.05.007.

Gosselin, M., M. Levasseur, P. A. Wheeler, R. A. Horner, and B. C. Booth (1997), New measurements of phytoplankton and ice algal production in the Arctic Ocean, *Deep Sea Res. Part II*, *44*(8), 1623–1644, doi:10.1016/S0967-0645(97)00054-4.

Guay, C. K., and K. Kenison Falkner (1997), Barium as a tracer of Arctic halocline and river waters, *Deep Sea Res. Part II*, *44*(8), 1543–1569, doi:10.1016/S0967-0645(97)00066-0.

Harms, I. H., M. J. Karcher, and D. Dethleff (2000), Modelling Siberian river runoff–Implications for contaminant transport in the Arctic Ocean, *J. Mar. Syst.*, *27*(1–3), 95–115, doi:10.1016/S0924-7963(00)00062-2.

Hölemann, J. A., M. Schirmacher, and A. Prange (2005), Seasonal variability of trace metals in the Lena River and the southeastern Laptev Sea: Impact of the spring freshet, *Global Planet. Change*, *48*(1–3), 112–125, doi:10.1016/j.gloplacha.2004.12.008.

Holmes, R. M., J. W. McClelland, B. J. Peterson, I. A. Shiklomanov, A. I. Shiklomanov, A. V. Zhulidov, V. V. Gordeev, and N. N. Bobrovitskaya (2002), A circumpolar perspective on fluvial sediment flux to the Arctic Ocean, *Global Biogeochem. Cycles*, *16*(4), 1098, doi:10.1029/2001GB001849.

Johnson, K. S., R. M. Gordon, and K. H. Coale (1997), What controls dissolved iron concentrations in the world ocean?, *Mar. Chem.*, *57*(3–4), 137–161, doi:10.1016/S0304-4203(97)00043-1.

Jones, E. P., L. G. Anderson, and J. H. Swift (1998), Distribution of Atlantic and Pacific waters in the upper Arctic Ocean: Implications for circulation, *Geophys. Res. Lett.*, *25*(6), 765–768, doi:10.1029/98GL00464.

Jones, E. P., L. G. Anderson, S. Jutterström, L. Mintrop, and J. H. Swift (2008), Pacific freshwater, river water and sea ice meltwater across Arctic Ocean basins: Results from the 2005 Beringia Expedition, *J. Geophys. Res.*, *113*, C08012, doi:10.1029/2007JC004124.

Klunder, M. B., P. Laan, R. Middag, H. J. W. de Baar, and J. C. van Ooijen (2011), Dissolved iron in the Southern Ocean (Atlantic sector), *Deep Sea Res. Part Part II*, *58*, 2678–2694, doi:10.1016/j.dsr2.2010.10.042.

Lannuzel, D., V. Schoemann, J. de Jong, L. Chou, B. Delille, S. Becquevort, and J.-L. Tison (2008), Iron study during a time series in the western Weddell pack ice, *Mar. Chem.*, *108*(1–2), 85–95, doi:10.1016/j.marchem.2007.10.006.

Martin, J. H., and R. M. Gordon (1988), Northeast Pacific iron distributions in relation to phytoplankton productivity, *Deep Sea Res. Part A*, *35*(2), 177–196, doi:10.1016/0198-0149(88)90035-0.

Measures, C. I. (1999), The role of entrained sediments in sea ice in the distribution of aluminium and iron in the surface waters of the Arctic Ocean, *Mar. Chem.*, *68*(1–2), 59–70, doi:10.1016/S0304-4203(99)00065-1.

Middag, R., H. J. W. de Baar, P. Laan, and K. Bakker (2009), Dissolved aluminium and the silicon cycle in the Arctic Ocean, *Mar. Chem.*, *115*(3–4), 176–195, doi:10.1016/j.marchem.2009.08.002.

Middag, R., P. Laan, H. J. W. de Baar, M. B. Klunder (2011), Fluvial and hydrothermal input of manganese into the Arctic Ocean, *Geochim. Cosmochim. Acta*, *75*, 2393–2408, doi:10.1016/j.gca.2011.02.011.

Moore, J. K., and O. Braucher (2008), Sedimentary and mineral dust sources of dissolved iron to the world ocean, *Biogeosciences*, *5*(3), 631–656, doi:10.5194/bg-5-631-2008.

Moore, R. M. (1983), The relationship between distributions of dissolved cadmium, iron and aluminium and hydrography in the central Arctic Ocean, in *Trace Metals in Sea Water*, edited by C. S. Wong et al., pp. 131–142, Plenum, New York.

Nürnberg, D., I. Wollenburg, D. Dethleff, H. Eicken, H. Kassens, T. Letzig, E. Reimnitz, and J. Thiede (1994), Sediments in Arctic sea ice: Implications for entrainment, transport and release, *Mar. Geol.*, *119*(3–4), 185–214, doi:10.1016/0025-3227(94)90181-3.

Östlund, H. G., and G. Hut (1984), Arctic Ocean water mass balance from isotope data, *J. Geophys. Res.*, *89*(C4), 6373–6381, doi:10.1029/JC089iC04p06373.

Pabi, S., G. L. van Dijken, and K. R. Arrigo (2008), Primary production in the Arctic Ocean, 1998–2006, *J. Geophys. Res.*, *113*, C08005, doi:10.1029/2007JC004578.

Rember, R. D., and J. H. Trefry (2004), Increased concentrations of dissolved trace metals and organic carbon during snowmelt in rivers of the Alaskan arctic, *Geochim. Cosmochim. Acta*, *68*(3), 477–489, doi:10.1016/S0016-7037(03)00458-7.

Rintoul, S., C. W. Hughes, and D. Olbers (2001), The Antarctic Circumpolar Current system, in *Ocean Circulation and Climate: Observing and Modelling the Global Ocean*, *Int. Geophys. Ser.*, vol. 77, edited by J. C. Gerold Siedler and G. John, chap. 4.6, pp. 271–302, Academic, San Diego, Calif.

Rudels, B. (2001), Ocean current: Arctic Basin circulation, in *Encyclopedia of Ocean Sciences*, edited by J. H. Steele, S. A. Thorpe, and K. K. Turekian, pp. 177–187, Academic, San Diego, Calif.

Rudels, B., E. P. Jones, U. Schauer, and P. Eriksson (2004), Atlantic sources of the Arctic Ocean surface and halocline waters, *Polar Res.*, *23*(2), 181–208, doi:10.1111/j.1751-8369.2004.tb00007.x.

Sedwick, P. N., and G. R. DiTullio (1997), Regulation of algal blooms in Antarctic shelf waters by the release of iron from melting sea ice, *Geophys. Res. Lett.*, *24*(20), 2515–2518, doi:10.1029/97GL02596.

Serreze, M. P., A. P. Barrett, A. G. Slater, R. A. Woodgate, K. Aagaard, R. B. Lammers, M. Steele, R. Moritz, M. Meredith, and C. M. Lee (2006), The large-scale freshwater cycle of the Arctic, *J. Geophys. Res.*, *111*, C11010, doi:10.1029/2005JC003424.

Spreen, G., and L. Kaleschke (2008), AMSR-E ASI 6.25 km Sea-Ice Concentration Data V5.4, http://www.ifm.zmaw.de/en/research/remote-sensing-assimilation/sea-ice/amsr-e-sea-ice-concentration/#c4255, Univ. Hamburg, Hamburg, Germany.

Steele, M., and T. Boyd (1998), Retreat of the cold halocline layer in the Arctic Ocean, *J. Geophys. Res.*, *103*(C5), 10,419–10,435, doi:10.1029/98JC00580.

Takata, H., et al. (2004), Spatial variability of iron in the surface water of the northwestern North Pacific Ocean, *Mar. Chem.*, *86*(3–4), 139–157, doi:10.1016/j.marchem.2003.12.007.

Thuroczy, C.-E., L. J. A. Gerringa, M. Klunder, P. Laan, M. Le Guitton, H. J. W. de Baar (2011), Distinct trends in the speciation of iron between the shallow shelf seas and the deep basins of the Arctic Ocean, *J. Geophys. Res.*, *116*, C10009, doi:10.1029/2010JC006835.

Tovar-Sanchez, A., C. M. Duarte, S. Hernández-León, and S. A. Sañudo-Wilhelmy (2009), Impact of submarine hydrothermal vents on the metal composition of krill and its excretion products, *Mar. Chem.*, *113*(1–2), 129–136, doi:10.1016/j.marchem.2009.01.010.

van der Merwe, P., D. Lannuzel, C. A. M. Nichols, K. Meiners, P. Heil, L. Norman, D. N. Thomas, and A. R. Bowie (2009), Biogeochemical observations during the winter-spring transition in east Antarctic sea ice: Evidence of iron and exopolysaccharide controls, *Mar. Chem.*, *115*(3–4), 163–175, doi:10.1016/j.marchem.2009.08.001.

Woodgate, R. A., K. Aagaard, and T. J. Weingartner (2005), A year in the physical oceanography of the Chukchi Sea: Moored measurements from autumn 1990–1991, *Deep Sea Res. Part II*, *52*(24–26), 3116–3149, doi:10.1016/j.dsr2.2005.10.016.

Yamamoto-Kawai, M., N. Tanaka, and S. Pivovarov (2005), Freshwater and brine behaviors in the Arctic Ocean deduced from historical data of δ^{18}O and alkalinity (1929–2002 A.D.), *J. Geophys. Res.*, *110*, C10003, doi:10.1029/2004JC002793.

Yamamoto-Kawai, M., E. Carmack, and F. McLaughlin (2006), Nitrogen balance and Arctic throughflow, *Nature*, *443*(7107), 43, doi:10.1038/443043a.

Yamamoto-Kawai, M., F. A. McLaughlin, E. C. Carmack, S. Nishino, and K. Shimada (2008), Freshwater budget of the Canada Basin, Arctic Ocean, from salinity, δ^{18}O, and nutrients, *J. Geophys. Res.*, *113*, C01007, doi:10.1029/2006JC003858.

D. Bauch, Ocean Circulation and Climate Dynamics, GEOMAR, Helmholtz Centre for Ocean Research, Wischhofstr. 1-3, Kiel D-24148, Germany.

H. J. W. de Baar and S. van Heuven, Department of Ocean Ecosystems, University of Groningen, Groningen NL-9750 AA, Netherlands.

M. B. Klunder and P. Laan, Biological Oceanography, Netherland Institute for Sea Research, Landsdiep 4, Den Burg NL-1797 SZ, Netherlands. (maarten.klunder@nioz.nl)

S. Ober, Physical Oceanography, Netherland Institute for Sea Research, PO Box 59, Den Berg NL-1790 AB, Netherlands.